

# Retrieval of greenhouse gases from GOSAT and greenhouse gases and carbon monoxide from GOSAT-2 using the FOCAL algorithm

Stefan Noël<sup>1</sup>, Maximilian Reuter<sup>1</sup>, Michael Buchwitz<sup>1</sup>, Jakob Borchardt<sup>1</sup>, Michael Hilker<sup>1</sup>, Oliver Schneising<sup>1</sup>, Heinrich Bovensmann<sup>1</sup>, John P. Burrows<sup>1</sup>, Antonio Di Noia<sup>2</sup>, Robert J. Parker<sup>2,3</sup>, Hiroshi Suto<sup>4</sup>, Yukio Yoshida<sup>5</sup>, Matthias Buschmann<sup>1</sup>, Nicholas M. Deutscher<sup>6</sup>, Dietrich G. Feist<sup>7,8,9</sup>, David W. T. Griffith<sup>6</sup>, Frank Hase<sup>10</sup>, Rigel Kivi<sup>11</sup>, Cheng Liu<sup>12</sup>, Isamu Morino<sup>5</sup>, Justus Notholt<sup>1</sup>, Young-Suk Oh<sup>13</sup>, Hirofumi Ohyama<sup>5</sup>, Christof Petri<sup>1</sup>, David F. Pollard<sup>14</sup>, Markus Rettinger<sup>15</sup>, Coleen Roehl<sup>16</sup>, Constantina Rousogonous<sup>17</sup>, Mahesh Kumar Sha<sup>18</sup>, Kei Shiomi<sup>4</sup>, Kimberly Strong<sup>19</sup>, Ralf Sussmann<sup>15</sup>, Yao Té<sup>20</sup>, Voltaire A. Velazco<sup>6,21</sup>, Mihalis Vrekoussis<sup>17,1,22</sup>, and Thorsten Warneke<sup>1</sup>

<sup>1</sup>Institute of Environmental Physics, University of Bremen, FB 1, P.O. Box 330440, 28334 Bremen, Germany

<sup>2</sup>Earth Observation Science, University of Leicester, LE1 7RH, Leicester, UK

<sup>3</sup>National Centre for Earth Observation, University of Leicester, UK

<sup>4</sup>Japan Aerospace Exploration Agency (JAXA), 305-8505, Tsukuba, Japan

<sup>5</sup>National Institute for Environmental Studies (NIES), Onogawa 16-2, Tsukuba, Ibaraki 305-8506, Japan

<sup>6</sup>Centre for Atmospheric Chemistry, School of Earth, Atmospheric and Life Sciences, University of Wollongong NSW 2522 Australia

<sup>7</sup>Max Planck Institute for Biogeochemistry, 07745 Jena, Germany

<sup>8</sup>Deutsches Zentrum für Luft- und Raumfahrt, Institut für Physik der Atmosphäre, 82234 Oberpfaffenhofen, Germany

<sup>9</sup>Ludwig-Maximilians-Universität München, Lehrstuhl für Physik der Atmosphäre, 80539 Munich, Germany

<sup>10</sup>Karlsruhe Institute of Technology, IMK-ASF, 76021 Karlsruhe, Germany

<sup>11</sup>Finnish Meteorological Institute, Space and Earth Observation Centre, Tähteläntie 62, 99600 Sodankylä, Finland

<sup>12</sup>Department of Precision Machinery and Precision Instrumentation, University of Science and Technology of China, 230026 Hefei, China

<sup>13</sup>Global Atmosphere Watch Team, Innovative Meteorological Research Department, National Institute of Meteorological Sciences, 3, Seohobuk-ro, Seogwipo-si, Jeju-do, Republic of Korea

<sup>14</sup>National Institute of Water and Atmospheric Research Ltd (NIWA), Lauder, Private Bag 50061, Omakau 9352, New Zealand

<sup>15</sup>Karlsruhe Institute of Technology, IMK-IFU, 82467 Garmisch-Partenkirchen, Germany

<sup>16</sup>California Institute of Technology, Global Environmental Center, Pasadena, CA 91125, USA

<sup>17</sup>Climate and Atmosphere Research Center (CARE-C), The Cyprus Institute, Nicosia, Cyprus

<sup>18</sup>Royal Belgian Institute for Space Aeronomy (BIRA-IASB), 1180 Brussels, Belgium

<sup>19</sup>Department of Physics, University of Toronto, Toronto, ON, M5S 1A7, Canada

<sup>20</sup>Laboratoire d'Etudes du Rayonnement et de la Matière en Astrophysique et Atmosphères (LERMA-IPSL), Sorbonne Université, CNRS, Observatoire de Paris, PSL Université, 75005 Paris, France

<sup>21</sup>Deutscher Wetterdienst, Meteorological Observatory, 82383 Hohenpeissenberg, Germany

<sup>22</sup>Center of Marine Environmental Sciences (MARUM), University of Bremen, Germany

**Correspondence:** S. Noël (stefan.noel@iup.physik.uni-bremen.de)

## Abstract.

Recently, the Fast atmospheric trace gas retrieval (FOCAL) algorithm has been applied to measurements of the Greenhouse gases Observing SATellite (GOSAT) and its successor GOSAT-2. FOCAL has been originally developed for Orbiting

Carbon Observatory 2 (OCO-2) retrievals with the focus on the derivation of carbon dioxide ( $\text{XCO}_2$ ). However, depending on the available spectral windows, FOCAL also successfully retrieves total column amounts for other atmospheric species. Here, we show new results from updated GOSAT and GOSAT-2 FOCAL retrievals. The main focus is placed on methane ( $\text{XCH}_4$ ; full physics and proxy product), water vapour ( $\text{XH}_2\text{O}$ ) and the relative ratio of semi-heavy water (HDO) to water vapour ( $\delta\text{D}$ ). Due to the extended spectral range of GOSAT-2 it is also possible to derive information on carbon monoxide ( $\text{XCO}$ ) and nitrous oxide ( $\text{N}_2\text{O}$ ) for which we also show first results. We also present an update on  $\text{XCO}_2$  from both instruments.

Compared to the previous product version (v1), the number of valid  $\text{XCO}_2$  data could be significantly increased in the updated version (v3.0) by 50% for GOSAT and about a factor of two for GOSAT-2. All FOCAL data products show reasonable spatial distribution and temporal variations. Comparisons with TCCON (Total Carbon Column Observing Network) result in station-to-station biases which are generally in line with the reported TCCON uncertainties.

With this updated version of the GOSAT-2 FOCAL data, we provide a first total column average  $\text{XN}_2\text{O}$  product. Global  $\text{XN}_2\text{O}$  maps show a gradient from the tropics to higher latitudes in the order of 15 ppb, which can be explained by variations in tropopause height. The new GOSAT-2  $\text{XN}_2\text{O}$  product compares well with TCCON. Its station-to-station variability is lower than 2 ppb, which is about the magnitude of the typical  $\text{N}_2\text{O}$  variations close to the surface. However, both GOSAT-2 and TCCON measurements show that the seasonal variations in the total column average  $\text{XN}_2\text{O}$  are in the order of 8 ppb peak-to-peak, which can be easily resolved by the GOSAT-2 FOCAL data.

## 1 Introduction

Global, long-term data sets of atmospheric constituents are essential to improve our understanding of the behavior of the Earth's atmosphere. Remote sensing by satellite instruments provides a way to derive large scale information from measurements. In a time of changing climate, reliable remote sensing data products gain importance, as they are a crucial input, e.g. for models used for climate projections and air quality simulations. Information about the global distribution of greenhouse gases and about their sources and sinks plays an important role in this context.

Several retrieval methods exist for the derivation of atmospheric information from satellite measurements. In many cases these approaches are based on spectral information from different wavelength regions, and they concentrate on, and are optimised for, a single product. However, the derivation of a specific product usually requires the consideration of various additional atmospheric constituents and processes.

Recently, Noël et al. (2021) presented a first version (v1.0) of a  $\text{XCO}_2$  data product from GOSAT (Greenhouse gases Observing SATellite; Kuze et al., 2009, 2016) and GOSAT-2 (Suto et al., 2021) measurements in the near-infrared (NIR) and shortwave infrared (SWIR) spectral regions derived with the FOCAL (Fast atmospheric trace gas retrieval) method (Reuter et al., 2017a, b). FOCAL is based on a full-physics retrieval in which scattering is approximated by a single layer. The Noël et al. (2021) paper focused on the  $\text{XCO}_2$  results, but the application of FOCAL to the GOSAT instruments includes the determination of various other atmospheric quantities. In the current paper, we present results from an updated version (v3.0) of the GOSAT and GOSAT-2 FOCAL retrieval. Although we will also show the results for the new  $\text{XCO}_2$  data, the main focus of

the paper is on the presentation and initial validation of the additional quantities that can be derived with a single retrieval, thus showing the capabilities of the FOCAL method beyond XCO<sub>2</sub>. In the following, in addition to XCO<sub>2</sub>, we present the GOSAT and GOSAT-2 FOCAL results for methane (XCH<sub>4</sub>; full physics and proxy product), water vapour (XH<sub>2</sub>O) and semi-heavy water (HDO, respectively its ratio to H<sub>2</sub>O denoted as  $\delta$ D). For GOSAT-2, we will also show results for carbon monoxide (XCO) and first nitrous oxide (XN<sub>2</sub>O) data.

~~For some of the gases derived from GOSAT measurements, several data products exist.~~ The Japanese National Institute for Environmental Studies (NIES) provides operational XCO<sub>2</sub>, XCH<sub>4</sub> (Yoshida et al., 2013) and XH<sub>2</sub>O products (Dupuy et al., 2016). NASA also released a XCO<sub>2</sub> product based on the ACOS retrieval, recently described by Taylor et al. (2022). A precursor of the FOCAL XCO<sub>2</sub> product v1.0 from Noël et al. (2021) is the BESD v01.04 product, also from the Institute of Environmental Physics (IUP) Bremen (Heymann et al., 2015). This is a near-real-time product produced for the Copernicus Atmospheric Monitoring Service (CAMS, <https://atmosphere.copernicus.eu/> (last access: 30-July-2020)). ~~It is planned to replace this~~ with a near-real-time version of the FOCAL XCO<sub>2</sub> product described in this paper in the near future. Several GOSAT products are produced for the Copernicus Climate Change Service (C3S, <https://climate.copernicus.eu/>; last access: 30-July-2020). In this context, the Netherlands Institute for Space Research (SRON) provides XCO<sub>2</sub> and XCH<sub>4</sub> data (Butz et al., 2011; Schepers et al., 2012). Similar products are also generated by the University of Leicester (Cogan et al., 2012; Parker et al., 2011, 2020). The ratio of HDO to H<sub>2</sub>O ( $\delta$ D) was derived by Frankenberg et al. (2013) and Boesch et al. (2013).


For GOSAT-2, operational XCO<sub>2</sub>, XCH<sub>4</sub>, XCO and XH<sub>2</sub>O SWIR products have been released by NIES (see <https://prdct.gosat-2.nies.go.jp/>, last visited 6 June 2021). There is no XN<sub>2</sub>O product for GOSAT-2 available yet.

The main aim of the current study is to give an overview of the large number of newly available FOCAL data products for GOSAT and GOSAT-2. To get an impression about the quality of these products, we compare them with ground-based measurements from the Total Carbon Column Observing Network (TCCON; Wunch et al., 2011). For GOSAT we also include comparisons with other available XCO<sub>2</sub> and XCH<sub>4</sub> GOSAT data sets.

The paper is structured as follows: After this introduction, we present the input data used in this study in section 2. We then describe the updated retrieval algorithm in section 3, followed by the results of the study (including first validation) in section 4. Finally, we summarise everything in the conclusions (section 5). Additional information is given in the appendix.

## 2 Input Data

The input data used in this study are essentially the same as for the v1.0 product described in Noël et al. (2021) with some updates described in the following.

 input spectra, we use calibrated GOSAT and GOSAT-2 L1B radiances of the three NIR/SWIR bands at around 0.76, 1.6 and 2.0  $\mu$ m. All data until the end of 2020 are processed. For GOSAT, we use product version V220.220, extended by V230.230 for about the last two months of 2020. The GOSAT-2 L1B product version is now V102.102. The instrumental line shape (ILS) data are the same as in Noël et al. (2021).

The solar irradiance and solar induced fluorescence (SIF) reference spectra are unchanged. The cross sections have been updated; we now use data from HITRAN2016 (Gordon et al., 2017, downloaded on 23 March 2021) in combination with updated cross sections from the NASA (National Aeronautics and Space Administration) ACOS/OCO-2 project, i.e. ABSCO v5.1 data (Benner et al., 2016; Devi et al., 2016).

As in Noël et al. (2021), surface properties are obtained from the Global Multi-resolution Terrain Elevation Data (GMTED2010; Danielson and Gesch, 2011) of the U.S. Geological Survey (USGS) and the National Geospatial-Intelligence Agency (NGA). Meteorology is taken from ECMWF (European Centre for Medium-range Weather Forecasts) ERA5 model data (Hersbach et al., 2020).

There has been a change in the a priori profile data used for  $\text{XCO}_2$  and  $\text{XCH}_4$ . These are now derived using a Simple cLimatological Model for atmospheric  $\text{CO}_2$  and  $\text{CH}_4$ , respectively, called SLIMCO2 and SLIMCH4 (see Appendix A for details). All other a priori data and the related uncertainties are unchanged compared to v1.0. The SLIMCO2 and SLIMCH4 data are also used in the bias correction for  $\text{XCO}_2$  and  $\text{XCH}_4$ . As “truth”, we use a subset of the SLIM data from 2019 that has been selected based on a comparison with TCCON data (see Noël et al., 2021, for a detailed description).

~~We still use the same TCCON data version GGG2014 for comparison,~~ but now for the extended time period until the end of 2020. All involved TCCON stations and related references are listed in Table 1.

In addition to the validation with ground-based data we also include comparisons with other GOSAT data sets for  $\text{XCO}_2$  and  $\text{XCH}_4$ , namely the ACOS v9r  $\text{XCO}_2$  product from NASA (Taylor et al., 2022); the full physics and proxy products from the University of Leicester (UoL  $\text{XCO}_2$  and  $\text{XCH}_4$  FP v7.3, UoL  $\text{XCH}_4$  proxy v9.0; Cogan et al., 2012); the full physics and proxy products from SRON (RemoTeC FP  $\text{XCO}_2$  and  $\text{XCH}_4$  v2.3.8, RemoTeC  $\text{XCH}_4$  proxy product v2.3.9; Butz et al., 2011); and the operational bias-corrected GOSAT  $\text{XCO}_2$  and  $\text{XCH}_4$  products from NIES v02.9x (Yoshida et al., 2013).

### 3 Retrieval Algorithm

The retrieval used in this study is a three-step approach consisting of pre-processing, processing and post-processing. Since the retrieval method is essentially the same as the one described in Noël et al. (2021) for product version 1.0 we will describe in the following only the differences applied for the updated product version (v3.0; v2 was an unreleased internal version). Most relevant changes for the current product version were in the pre- and post-processing parts.

#### 3.1 Pre-Processing

The pre-processing collects and prepares all data required for the processing. This step especially includes the measured GOSAT and GOSAT-2 spectra, and geolocation and matching meteorological and topographic information (from ECMWF ERA5 and GMTED2010). Furthermore, some initial filtering (especially for clouds) is performed for the new FOCAL products, some filter limits of the pre-processing have been relaxed to increase final the data yield: We now use a maximum solar zenith angle of  $90^\circ$  and also latitudes up to  $\pm 90^\circ$  in v1.0, both limits were set to  $70^\circ$ . Note that these limits are applied for pre-processing; further filtering is done later during post-processing, depending on the different products (see section 3.3). All

other filtering (including the cloud filter) is unchanged compared to v1.0. The main difference in pre-processing to v1.0 is, therefore, that for v3.0 high latitudes are not necessarily filtered out before processing. Furthermore, as mentioned above, we now use SLIMCO2 and SLIMCH4 data as a priori for XCO<sub>2</sub> and XCH<sub>4</sub>.

### 3.2 Processing



405 The processing for v3.0 is very similar to the one of v1.0. It is based on the Fast atmospheric trace gas retrieval (FOCAL) algorithm described in Reuter et al. (2017b). We now use a modified version of FOCAL, which assumes isotropic instead of Lambertian scattering at the scattering layer. The fitting windows are the same as in v1.0, but we also fit H<sub>2</sub>O in the NIR band (see Tab. 2).

The state vector elements (see Tab. 3) are also almost the same as in v1.0; however, we increased the degrees of the background polynomials to improve the fit residuals such that now all fitted polynomials are of degree 3 except for the small solar induced fluorescence (SIF) windows where we use a degree of 1 and the XN<sub>2</sub>O window where a degree of 4 is used.

All quantities in the state vector are retrieved simultaneously. For CO<sub>2</sub>, CH<sub>4</sub> and H<sub>2</sub>O we derive profiles on 5 layers which are then converted to total column average  $\delta D$ , XCO and XN<sub>2</sub>O are derived via scaling factors. The XCH<sub>4</sub> proxy product is derived after the retrieval from these full physics products (see below). In the case of GOSAT-2, all scattering parameters as well as methane, water vapour and  $\delta D$  are only fitted in windows 1 to 6 (i.e. those spectral ranges which are also available for GOSAT). This is done for consistency reasons.

As in v1.0, before the retrieval for GOSAT – but not GOSAT-2 – we compute a spectral correction factor to account for changes in the spectral calibration with time. This factor is now obtained from the spectral difference of Fraunhofer lines in the solar irradiance and measured radiance in the SIF window, which is more stable than the least-squares fitting procedure used in v1.0. This new method only corrects for shifts on the scale of one spectral sampling interval (0.2 cm<sup>-1</sup>); this, however, is sufficient, as additional spectral shift and squeeze factors are determined in the later retrieval.

We also use a noise model to correct the uncertainties of the GOSAT and GOSAT-2 spectra estimated during pre-processing and consider possible forward model uncertainties in the retrieval. This noise model is the same as in v1.0, but we re-computed the parameters for all fitting windows based on an input data set consisting of one day per month in 2019 for both GOSAT and GOSAT-2. The resulting parameters are, however, similar for v1.0 and v3.0.

### 3.3 Post-Processing

The main changes between v1.0 and v3.0 occur in the post-processing. The overall concept of our new approach is that we tried to establish a generic, mostly automated procedure that provides reproducible results and thus can be applied to all gases under consideration. However, it still allows for an optimisation for each product.

130 The following post-processing steps are in general applied to all products:

1. Basic filtering.
2. Quality filtering.

### 3. Bias correction (for CO<sub>2</sub> and CH<sub>4</sub> only)

Note that, in contrast to v1.0, there is no longer a filter on the derived bias applied after the bias correction.

135 The XCH<sub>4</sub> proxy product is computed during post-processing from:

$$\text{XCH}_4^{\text{proxy}} = \text{XCH}_4^{\text{retrieved}} \frac{\text{XCO}_2^{\text{apriori}}}{\text{XCO}_2^{\text{retrieved}}} \quad (1)$$

This means we normalise the retrieved full physics XCH<sub>4</sub> by the retrieved full physics XCO<sub>2</sub> (both without bias correction) and use as reference the a priori XCO<sub>2</sub>. Note that this is different to e.g. the SRON XCH<sub>4</sub> proxy product (Wu et al., 2021), which is derived from a dedicated non-scattering retrieval using a different wavelength region (6045 – 6138 cm<sup>-1</sup>). The uncertainty of the proxy product is then determined via error propagation. The XCH<sub>4</sub> proxy product is then treated in post-processing as the other products.

#### 3.3.1 Basic filtering

In contrast to v1.0, the basic filtering does not involve filtering based on scientific knowledge, e.g. by using pre-described limits of scattering parameters or product uncertainties. This is no longer done as these fixed limits removed too many possibly valid data points, especially in the case of GOSAT-2.

Therefore, the basic filtering now only includes the filtering for good convergence ( $\chi^2$  smaller than 2) and a maximum residual-to-signal ratio (RSR) as a function of the noise-to-signal ratio (NSR). This is done in the same way as for v1.0 (see Noël et al., 2021), but with the updated noise model parameters mentioned above. This part of the basic filtering is common for all products.

150 For GOSAT, the RSR filters for all fitting windows (1–6) are applied to all data products. In case of GOSAT-2, for consistency reasons, we also apply only the RSR filters for windows 1–6 to those products, that are also available from GOSAT (i.e. XCO<sub>2</sub>, methane and water vapour products). For the others, i.e. XCO and XN<sub>2</sub>O, we only apply RSR filters from the NIR (windows 1 and 2, where most of the scattering information comes from) and those windows where these gases are retrieved, namely window 8 for XCO and window 7 for XN<sub>2</sub>O. This is to avoid that e.g. a valid XCO<sub>2</sub> measurement is filtered out due to a bad XN<sub>2</sub>O fit (or vice versa).

In addition to this, we apply a filter on a maximum solar zenith angle (SZA) of 75° because we cannot expect good data products for too low lighting conditions. This SZA filter is applied for all products except for water vapour, because requirements on water vapour are not as strict as e.g. for XCO<sub>2</sub>. This is why we do not apply this strict filter already in pre-processing (where we only limit the SZA to 90°, see above).

#### 160 3.3.2 Quality filtering

The quality filtering is product-specific, but follows the same strategy for each target gas. In general, we perform independent filtering for water and land surface.

Filtering out of low-quality data was done in v1.0 by a random forest filter. However, as explained in Noël et al. (2021), the performance of this filter method was limited as it essentially filtered out fewer data than expected. Therefore, we replaced

165 this filtering for v3.0 with a filter procedure that has already been successfully used in OCO-2 retrievals; details can be found in Reuter et al. (2017a). This procedure is based on a minimisation of the local variance. This is done by computing, for a subset of the data, the variance of the difference between the retrieved quantity and its median on a  $15^\circ \times 15^\circ$  grid.

Based on this subset, we check which variables from a given list of the candidate variables perform best in reducing the local variance when removing data corresponding to the highest or lowest 1% of each variable. This action defines a new upper or lower limit for this variable. We repeat this until a prescribed amount of data is removed. The output of this procedure is a list of “best” variables and their new filter limits.

This subset has been generated from data of 2019 for GOSAT and GOSAT-2, to which the basic quality filter as described above has been applied. Note that – in contrast to v1.0 – this subset no longer depends on the reference database used in the bias correction.

175 A general problem with this filtering method is that it tends to filter out values from regions with higher noise, which might result in reduced coverage at higher latitudes if too many data are to be filtered out.

Therefore, we apply this filtering in two steps: First, using the variance filter method, we only determine limits for (only) the scattering optical depth parameters derived in the retrieval for a given percentage of data to be filtered out ( $P_\tau$ ).

After applying this filter, we further reduce the number of data by another percentage ( $P_V$ ) by using the variance filter method again, but now for an extended list of possible filter candidates. This list of variables has been largely reduced compared to v1.0. It now only comprises results from the retrieval, namely the uncertainties (but not values) of the retrieved target species,  $\chi^2$ , scattering parameters and their uncertainties, the polynomial coefficients and their uncertainties, wavelength shift/squeeze and their uncertainties, and surface roughness. We explicitly no longer include geolocation / viewing geometry parameters and surface elevation to avoid that data are filtered out due to e.g. a specific geographical region. The retrieved  $\text{CO}_2$  gradient at the surface is also not used anymore, as this might result in filtering out scenes with too high  $\text{CO}_2$  in the boundary layer close to a point source. However, because of the large number of fitting windows this still leaves a list of about 200 possible parameters. To reduce this to a reasonable number, we run this variance filter twice: first, with the full list, then with only the best 10 parameters. This number of 10 parameters is only an upper limit, which has been chosen by checking that adding more parameters does not further reduce the variance significantly. Depending on the relevance of individual quantities even fewer parameters are needed in some cases.

The choice of the number of data to be filtered out is – as always – a trade-off between the remaining number of data points and data quality. For the v3.0 data, we determined suitable numbers for  $P_\tau$  and  $P_V$  by looking at the resulting data quality (maps and validation) for different settings. As for the SZA filter, the optical depth filter is not applied for each product. We use the same values for GOSAT and GOSAT-2; these are listed in Tab. 4. The finally selected filter variables and their limits are specific for each product, surface and instrument. They are given in the Appendix in Tab. A1 to A12.

### 3.3.3 Bias correction

After filtering out data as described above, we apply a bias correction to  $\text{XCO}_2$  and the  $\text{XCH}_4$  full physics and proxy products. The overall procedure is the same as described in detail in Noël et al. (2021). The bias correction is based on a random



forest regression using, as for v1.0, the ten most relevant parameters and a random forest database as input. These have been  
 200 determined as described in Noël et al. (2021), using as input the variance-filtered test subset of data as mentioned above  
 and a reference database giving the “true”  $\text{XCO}_2$  and  $\text{XCH}_4$ . This reference database has been generated from a subset of  
 daily SLIMCO2 and SLIMCH4 data (see Appendix A) for 2019, which agree within  $\pm 0.5$  ppm for  $\text{XCO}_2$  and  $\pm 10$  ppb for  
 $\text{XCH}_4$  with corresponding TCCON data. The “best” parameters have been chosen from essentially the same list of candidate  
 variables used in the variance filter, but now extended with surface elevation and type, solar zenith angle, viewing zenith angle,  
 205 continuum signal and flags for quality and instrument gain.

The final choice of bias correction parameters and their relevance is shown in Fig. A7 for GOSAT and Fig. A8 for GOSAT-2  
 (see Appendix B).

We also perform a correction of the retrieved  $\text{XCO}_2$  and  $\text{XCH}_4$  uncertainties via a linear function. The coefficients of this  
 function (see Tab. 5) are determined in a similar way as described in Noël et al. (2021), but instead of TCCON data we now  
 210 use data from the SLIMCO2/SLIMCH4 reference database as “true” values.

## 4 Results

All GOSAT and GOSAT-2 data until the end of 2020 have been processed. Fig. 1 shows the final number of valid FOCAL data  
 as a function of time for the different products. The numbers are different for each product because of the individual filtering  
 (see above). For comparison, the numbers for the v1.0  $\text{XCO}_2$  products are also shown. Fig. 1a compares the number of yearly  
 215 GOSAT-FOCAL  $\text{XCO}_2$  data with other available GOSAT data products from SRON, the University of Leicester (UoL), NIES  
 and NASA (ACOS product). A similar comparison is shown in Fig. 1b for  $\text{XCH}_4$  full physics and proxy products. The resulting  
 amount of data for the GOSAT-FOCAL water vapour products is shown in Fig. 1c. The yield of valid FOCAL products was  
 improved in v3.0 compared to v1.0. The number of valid FOCAL  $\text{XCO}_2$  and methane results exceeds those of all other GOSAT  
 data sets.

220 The total number of GOSAT-2 FOCAL products (see Fig. 1d) was also improved, but is still lower than for GOSAT. This  
 is because a larger fraction of data are already removed during the basic filtering due to larger residuals / less convergence.  
 This hints at possible issues with the radiometric calibration or an incomplete instrument model used by FOCAL, neglecting  
 important instrument features, e.g. currently unconsidered effects of remaining polarisation sensitivities of the instrument.

### 4.1 Global maps

225 For each of the different data products an example map comprising a mean for April 2019, gridded to  $5^\circ \times 5^\circ$ , is shown in  
 Fig. 2 for GOSAT and in Fig. 3 for GOSAT-2. In all maps, grid points that were only based on a single measurement have  
 been omitted to avoid outliers. The spatial patterns of methane, water vapour,  $\delta\text{D}$  and  $\text{XCO}_2$  look very similar for GOSAT and  
 GOSAT-2. GOSAT-2 data show in general fewer gaps over the oceans, but with smaller latitudinal coverage. The latter is due  
 to the currently applied RSR filtering for GOSAT-2, which especially removes data over water surfaces. Note that over the year  
 230 the spatial range of valid data varies according to illumination conditions.



The XCO<sub>2</sub> data show higher values in the northern than in the southern hemisphere as expected during spring time

For methane, the known source regions in the US, Africa and Asia are clearly visible, as well as the inter-hemispheric gradient. The spatial coverage of the proxy product is much larger than for the full physics product, especially at higher latitudes

235 Water vapour (XH<sub>2</sub>O) also shows the expected behaviour: large values in the tropics and lower values at higher latitudes. All  $\delta D$  values are in the expected range (about 0 to -300‰); they also decrease from the tropics to higher northern and southern latitudes. This is because water vapour generated in the tropics by strong evaporation is transported to higher latitudes, during which the heavier HDO decreases more rapidly via precipitation than H<sub>2</sub>O. The observed spatial distribution of  $\delta D$  is in line with the maps shown in Frankenberg et al. (2013).

240 For GOSAT-2 there are also data for carbon monoxide (XCO) and XN<sub>2</sub>O. In the XCO map the expected source regions in China, Indonesia and Africa (fossil fuel combustion, biomass burning) are apparent over the otherwise quite smooth and constant background. The transport of XCO from the equatorial African fire regions to the west over the Atlantic ocean due to the trade winds is clearly visible

The XN<sub>2</sub>O product shows an overall decrease of the background XN<sub>2</sub>O from the tropics to higher latitudes in the order of  
245 15 ppb. Such gradients were also observed by the IASI (Infrared Atmospheric Sounding Interferometer) instrument on Metop (Barret et al., 2021), however, we see larger differences. This could be related to the sampling of the XN<sub>2</sub>O data. Furthermore, the IASI data shown in Barret et al. (2021) refer to the mid-troposphere over the ocean only, whereas the GOSAT-2 FOCAL data are total column averages over all surfaces. The latitudinal XN<sub>2</sub>O gradient can, in principle, be explained by the variation of the tropopause height. As most of the XN<sub>2</sub>O is contained (and well mixed) in the troposphere, the total column average is  
250 larger in the tropics (where the tropopause is high) than at higher latitudes. We also see increased XN<sub>2</sub>O over central Africa. This is also visible in IASI data and probably related to convection (see Ricaud et al., 2009).

## 4.2 Time series

Time series of all GOSAT-FOCAL data products for different latitudinal regions are depicted in Fig. 4. These plots show the expected temporal behaviour: A seasonal cycle is visible in all data sets; amplitudes and/or phase differ for northern and  
255 southern latitudes with usually more variability in the north

The methane full physics and proxy products show a similar temporal variation with increasing XCH<sub>4</sub> (about 10 ppb per year, in line with recent annual changes from NOAA ground-based measurements, see [https://gml.noaa.gov/ccgg/trends\\_ch4/](https://gml.noaa.gov/ccgg/trends_ch4/) (last access 11 January 2022)). Small differences between the average XCH<sub>4</sub> full physics and the proxy products can be explained by the broader spatial coverage of the proxy product.

260 For water vapour (XH<sub>2</sub>O), the seasonal cycles in the northern and southern hemispheres are shifted by about six months, in line with the seasonal shift of the intertropical convergence zone (ITCZ). On the global scale, these seasonal variations largely average out. No clear trend is visible in the GOSAT water vapour column from 2009 to 2020

Average values of  $\delta D$  vary between about -180‰ and -120‰. As for water vapour, seasonal variations are small in the global average, but year-to-year variations in the seasonal cycle are large  $\delta D$ .

265 The GOSAT-2 time series (see Fig. 5) show similar temporal variations to the GOSAT data, but of course, they only cover the years 2019 and 2020. XCO shows similar values and seasonal variations for all latitudinal regions except for the southern hemisphere, where XCO is on average about 30 ppb lower than in the northern hemisphere, probably because most sources are around the equator or in the northern hemisphere extra-tropics.

The GOSAT-2 XN<sub>2</sub>O also shows some seasonal variations of up to about 8 ppb peak-to-peak. However, this seasonality is at least partly a sampling effect. The background XN<sub>2</sub>O, as shown in Fig. 3g, comprises larger values in the tropics than at higher latitudes. Because of the varying latitudinal coverage of GOSAT mean data throughout the year, the regions outside the tropics are not covered during all seasons, which introduces an apparent variation in the averages. This effect in principle applies to all data, but is especially pronounced for XN<sub>2</sub>O, for which other spatial variations are low. In the tropics, the XN<sub>2</sub>O data are always high, and the variations are much smaller. In fact, we see a slight increase in XN<sub>2</sub>O of about 1 ppb per year, which is about what is expected from ground-based measurements (see growth rate plots on the NOAA Global Monitoring Laboratory website; <https://gml.noaa.gov/hats/combined/N2O.html>, last access 30 June 2021). This result is also in line with IASI data (Barret et al., 2021).

### 4.3 TCCON comparisons

To assess the quality of the data, for each GOSAT and GOSAT-2 FOCAL product we perform a comparison with TCCON data using the same procedure as in Noël et al. (2021); see also Reuter et al. (2019, 2020) for details.

For most gases, we also use the same collocation criteria: a maximum time difference of 2 h, a maximum spatial distance of 500 km and a maximum surface elevation difference of 250 m between satellite and ground-based measurement. However, for water vapour and carbon monoxide these limits are reduced to 1 h time difference and 150 km spatial distance to account for their higher variability. We only include stations with a minimum of 50 data points.

285 For XCO<sub>2</sub> and XCH<sub>4</sub> we also perform comparisons with other available GOSAT products from SRON, the University of Leicester, NASA(ACOS) and NIES.

From the comparisons, we derive the following main quantities:

- The mean station bias, defined as the mean of all biases at each station; this can be interpreted as a global offset to all stations.
  - 290 – The station-to-station bias, defined as the standard deviation of the individual station biases. This can be interpreted as regional bias.
  - The mean scatter, defined as the square root of the mean of the variances at each station. This is a measure for the single sounding precision.
  - The seasonal bias, defined as the standard deviation (rms) of the seasonal variation of the difference FOCAL–TCCON at each station. This is equivalent to a temporal bias.
- 295

Figs. 6 to 10 show the resulting bias and scatter for each GOSAT and GOSAT-2 product and TCCON station. Example time series for the TCCON station Lamont (US) are shown in Figs. 11 and 12. This station was selected because it provides good temporal coverage of TCCON data also for the GOSAT-2 time frame (2019–2020). All results of the comparisons are summarised in Tab. 6.

300 The mean station bias is mainly given for reference, because it is usually not relevant for applications that are only interested in the spatial and temporal gradients of the gas (like for  $\text{XCO}_2$ ). The quantities station-to-station bias, seasonal bias, and mean scatter are more important as they describe the quality of regional and/or temporal gradients, which are, e.g., needed to quantify potential sources and sinks. The seasonal bias is derived from a trend model fit; therefore the corresponding values for GOSAT-2 are less reliable, because the time interval is only about two years. The number of stations and data points used in  
305 the comparison depends on the different products, the collocation criteria and the length of the time series. Therefore, there are many fewer collocations for GOSAT-2. The  $\text{XCH}_4$  proxy products, as well as the  $\text{XH}_2\text{O}$  and  $\text{XCO}$  products, have the largest number of collocations because of the relaxed filtering.

#### 4.3.1 $\text{XCO}_2$ results

For GOSAT FOCAL v3.0 the  $\text{XCO}_2$  station-to station bias is 0.51 ppm and the mean scatter 2.19 ppm. While the bias is  
310 slightly reduced, the scatter is slightly larger than the values for v1.0 (0.56 ppm, 1.89 ppm, see Noël et al., 2021). This higher scatter is still acceptable noting the increased number of data points, which always increases the scatter, and an estimated  $1-\sigma$  TCCON uncertainty of 0.4 ppm for  $\text{XCO}_2$ , see Wunch et al. (2010). Note that this relation between number of data and data points is due to the filtering, which is based on reducing the local variance by removing data points (see above). As stronger filtering therefore results in less data with a lower scatter.

315 FOCAL values are also in quite good agreement with those from the other data sets, but still do not reach the low bias and scatter of the NASA ACOS product (0.44 ppm and 1.66 ppm).

GOSAT-2  $\text{XCO}_2$  comparison results for v1.0 were considered less reliable because of the shortness of the time series (less than one year). For v3.0, we now have almost two years of data and, due to the updated product version, also a higher data yield, which results in almost 10 times more collocations with TCCON than in v1.0. We now get a station-to station bias of  
320 0.91 ppm, which is still slightly higher compared to GOSAT but lower than in v1.0 (1.14 ppm). For GOSAT-2, the biases are typically negative for southern stations and positive for northern stations. The derived mean scatter of 2.02 ppm is somewhat lower than the v3.0 GOSAT value and slightly higher than the v1.0 scatter for GOSAT-2 (1.89 ppm). As mentioned above, this is related to the different number of data points.

The derived seasonal bias is low (0.33 ppm for GOSAT, 0.62 ppm for GOSAT-2). The seasonal variations of the TCCON  
325 data at Lamont are well reproduced by the GOSAT and GOSAT-2 FOCAL data with no apparent offset, but the satellite data show a larger scatter (see Figs. 11a and 12a)

### 4.3.2 XCH<sub>4</sub> results

The full physics XCH<sub>4</sub> product for GOSAT has a station-to-station bias of 4.3 ppb, which is similar to the estimated 1- $\sigma$  TCCON uncertainty from Wunch et al. (2010) of 3.5 ppb and also compares well to the other data products. The value for the GOSAT FOCAL proxy product is 6.1 ppb, which is about 1–2 ppb higher than all other products but still in an acceptable range as it is better than the Copernicus systematic error threshold requirement of 10 ppb and close to the breakthrough requirement of better than 5 ppb (see Table 3 in Buchwitz et al., 2021). For GOSAT-2, we get a station-to-station bias of 4.7 ppb for the full physics XCH<sub>4</sub> product and 6.2 ppb for the proxy.

The mean scatter of the GOSAT and GOSAT-2 FOCAL XCH<sub>4</sub> product is around 12 ppb, which is slightly lower than for the other data products. The seasonal bias for all GOSAT and GOSAT-2 products is around 3 ppb. For both instruments, the temporal variations of the FOCAL full physics and proxy XCH<sub>4</sub> products agree well with the Lamont TCCON data (see Figs. 11b,c and 12b,c). In general, the FOCAL data are systematically lower by a few ppb, in line with the observed mean station bias of around -3–6 ppb, see Tab. 6.

### 4.3.3 XH<sub>2</sub>O results

Since water vapour is highly variable, the comparison results depend strongly on the involved TCCON stations. Because of the less strict filter criteria for XH<sub>2</sub>O there are typically more data (and collocations) at higher latitudes than for the other full physics products. We get a similar mean scatter of about 300 ppm for GOSAT and GOSAT-2 FOCAL XH<sub>2</sub>O. The station-to-station bias is 116 ppm for GOSAT and 152 ppm for GOSAT-2, which is even lower than the TCCON uncertainty of 200 ppm estimated by Wunch et al. (2010). The seasonal bias for GOSAT-2 is 110 ppm; for GOSAT it is even smaller (66 ppm). The derived station-to-station biases and mean scatter values are in line with results derived for the OCO-2 FOCAL product (206 ppm and 293 ppm, respectively, see Reuter et al., 2017a). As also mentioned there, these high values can at least partly be attributed to the large natural variability of water vapour. This variability can also be seen in the time series at Lamont (Figs. 11d and 12d), which show the same seasonal variations of around 4000 ppm peak-to-peak for all data sets.

### 4.3.4 $\delta$ D results

For  $\delta$ D we get station-to-station biases of only 8.6‰ for both instruments; the mean scatter is about 32‰ for GOSAT and GOSAT-2. The seasonal bias for GOSAT is 6‰, the GOSAT-2 value is 13‰. The mean station bias is quite large (around -83‰ for GOSAT and GOSAT-2). This is slightly larger than corresponding values between about -20‰ and -70‰ derived from a GOSAT–TCCON comparison performed by Boesch et al. (2013) for data between April 2009 and June 2011. Note that there is no uncertainty estimate available for the TCCON  $\delta$ D data, so all numbers given here should be treated with caution. The Lamont time series (Figs. 11e and 12e) show a systematic offset between TCCON on GOSAT/GOSAT-2 in line with the mean station bias, but the seasonality is well reproduced, although the satellite data show a larger scatter.

### 4.3.5 XCO results

XCO and XN<sub>2</sub>O products are only available for GOSAT-2, which covers a larger spectral range. The TCCON comparison for XCO reveals a station-to-station bias of 4.3 ppb, a mean scatter of 7.7 ppb and a seasonal bias of 2.8 ppb. In fact, the XCO bias and scatter varies strongly between the different TCCON stations (see Fig. 10) but the derived values agree quite well with the TCCON uncertainty for carbon monoxide of 2 ppb. The data at Lamont (Fig. 12f) show that the temporal variation of XCO is well captured by the FOCAL product, but there is a systematic offset in line with the mean station bias of about 15 ppb.

### 4.3.6 XN<sub>2</sub>O results

The FOCAL XN<sub>2</sub>O new data product that is so far not available from other GOSAT-2 retrievals. For XN<sub>2</sub>O we get from the TCCON comparison a station-to-station bias of 1.6 ppb and a mean scatter of 4.0 ppb. The seasonal bias is 1.6 ppb. Since the corresponding 1- $\sigma$  TCCON uncertainty from Wunch et al. (2010) is 1.5 ppb we consider this as a reasonable agreement. The values for XN<sub>2</sub>O are similar to the expected local XN<sub>2</sub>O variability of a few ppb (see e.g. García et al., 2018), but it should be considered that the total column average has a larger variability due to e.g. variations in tropopause height than surface data. This can be seen from Fig. 12g: Both TCCON and GOSAT-2 observe total column seasonal variations with peak-to-peak differences of about 8 ppb, in line with the time series results. There is no visible bias between TCCON and GOSAT-2, but the scatter of the GOSAT-2 data is larger.

## 5 Conclusions

An updated version (v3.0) of the FOCAL retrieval algorithm has been applied to GOSAT and GOSAT-2 measurements in the NIR and SWIR spectral regions. This results in a variety of trace gas products, all derived within one retrieval. For both GOSAT instruments we determine full physics products for methane, water vapour and  $\delta D$  as well as a proxy methane product in addition to XCO. For GOSAT-2, also carbon monoxide and a nitrous oxide product are retrieved.

Overall, the yield of valid data could be improved in GOSAT and GOSAT-2 FOCAL v3.0. The number of XCO<sub>2</sub> full physics data has increased by about 50% for GOSAT and has even doubled for GOSAT-2. This is mainly due to relaxations in the filtering of data and improved post-processing. The proxy methane, carbon monoxide and XH<sub>2</sub>O products even have about two times more data than the full physics products.

The spatial distribution of all gases and their temporal variation looks reasonable. For the new GOSAT-2 XN<sub>2</sub>O we observe a gradient between the tropics and higher latitudes of about 15 ppb which can be explained by variations in the tropopause height. A similar gradient has been seen in IASI data.

The new GOSAT and GOSAT-2 products have been compared with ground-based TCCON data to get a first quality assessment. All FOCAL data agree with TCCON within the uncertainties of both data sets.

The accuracy of the GOSAT-2 FOCAL  $\text{XN}_2\text{O}$  is in the order of a few ppb for a single sounding. We expect this to be improved by averaging of data, such that e.g. monthly or annually gridded products can provide interesting information about  $\text{XN}_2\text{O}$ , especially since there are not many global satellite measurements available for this species.

390 *Data availability.* The GOSAT and GOSAT-2 FOCAL v3.0 data sets are available on request from the authors.

## Appendix A: SLIMCO2 and SLIMCH4

The “Simple cLImatological Model for atmospheric  $\text{CO}_2$  or  $\text{CH}_4$ ” SLIMCO2 or SLIMCH4 has been developed to provide estimates of dry-air mole fraction profiles and column averages of atmospheric  $\text{CO}_2$  or  $\text{CH}_4$  with reasonable accuracy at minimum computational costs. A key application of SLIMCO2 or SLIMCH4 is to compute  $\text{CO}_2$  or  $\text{CH}_4$  a priori information  
395 for remote sensing algorithms which is why it provides also estimates of the corresponding error covariance matrix which can be used, e.g., by optimal estimation frameworks.

The climatology database of SLIMCO2 v2021 has been derived from 16 years (2003-2018) of  $\text{CO}_2$  mole fraction data of NOAA’s CarbonTracker model version CT2019B Jacobson et al. (2020). It has the same  $3^\circ \times 2^\circ$  spatial resolution as the used global CarbonTracker model fields. Temporally, it covers one year sampled in 36 time steps, corresponding to a grid  
400 resolution of about 10 days. The climatology database of SLIMCH4 v2021 has been derived from 13 years (2000-2012) of TM5-4DVAR  $\text{CH}_4$  mole fraction data (Bergamaschi et al., 2013) with a spatial resolution of  $6^\circ \times 4^\circ$ . Temporally, it is sampled in 36 time steps, just as the climatology database of SLIMCO2 v2021. Both databases feature a height grid with 20 layers. The height gridding is done in a way that each layer consists of the same number of dry-air particles so that the column-average can simply be computed by averaging the mole-fraction profile. When reading the climatology database, SLIM allows either  
405 nearest neighbour or trilinear interpolation in longitude, latitude, and ~~say~~ of year. Additionally, SLIM is able to convert the height gridding to the one that is used, e.g., for the FOCAL OCO-2  $\text{XCO}_2$  retrieval using five height layers for  $\text{CO}_2$ .

First, we computed the global mean XGAS ( $\text{XCO}_2$  or  $\text{XCH}_4$ ) from the corresponding model for each January 1st (00:00 UTC) in the covered time period. In the next step, we went through all model time steps of the analysed period and subtracted the global mean XGAS, assuming linear growth within the years. Finally, we created the climatology databases by incremen-  
410 tally computing the average and standard deviation of the gases mole-fraction of all growth corrected model time steps falling into the 10-days temporal grid-cells of the database. In this way, the created databases basically consist of growth-removed seasonal cycle anomalies.

In addition to the created 4D data fields, the database contains a table of annual growth rates obtained from NOAA (<https://gml.noaa.gov/ccgg/trends/gr.html>, last access 03.07.2021). Currently, the implemented table covers the time periods 1959-  
415 2020 for  $\text{CO}_2$  and 1984-2020 for  $\text{CH}_4$ , but it can be extended if needed to improve the quality of SLIM estimates in years before or after these periods. Fig. A1 shows the NOAA annual mean growth rates for  $\text{CO}_2$  and  $\text{CH}_4$  computed from global

marine surface data as stored in the database. As visible in the figure, the NOAA growth rate agrees well with the growth computed from the model data as described above.

In the following, we describe, how SLIM uses its database to estimate the  $\text{CO}_2$  or  $\text{CH}_4$  atmospheric dry-air mole fraction for a given longitude, latitude, and time. The database has been generated as follows: First, SLIM computes an estimate of the global average mole fraction by linear interpolation in the accumulated growth rates database. Note that extrapolation to dates outside of the spanned period is done by assuming a 10-years average growth rate (dashed lines in Fig. A1). This global average is added to the mole fraction anomaly interpolated from the corresponding 4D database field for the given longitude, latitude, and day of year.

Figures A2 shows examples of a global  $\text{XCO}_2$  and  $\text{XCH}_4$  map as read from the models (panels c and d) and in panels a and b the corresponding maps of SLIM XGAS values. Since the SLIM layers are defined such that ~~the~~ all contain the same number of dry air particles, the SLIM XGAS values can be computed as mean of all layer values. As one can also see in the difference maps (panels e and f), the large scale patterns such as north/south gradient are well reproduced and differences are mainly due the specific synoptic situation in the model field, which usually change from year to year and which, therefore, cannot be reproduced by a simple climatology. At the example of  $\text{CO}_2$ , the largest natural surface fluxes occur during the northern hemispheric growing season. Therefore, the largest deviations between CT2019B and SLIMCO2 occur in the northern hemisphere in Fig. A2e.

By comparing one million randomly selected profiles in the period 2003-2018, we computed that the SLIMCO2  $\text{XCO}_2$  is on average 0.1 ppm lower than the corresponding CarbonTracker values. ~~The standard deviation of the difference amounts 0.57 ppm and the correlation coefficient between both quantities is 0.998~~ (see Fig. A3a). The corresponding experiment for SLIMCH4 results in a mean difference of 3 ppb, a standard deviation of the difference of 7.2 ppb, and a correlation coefficient of 0.989 (see Fig. A3b).

The error covariance matrix for the 5-layered SLIMCO2 profiles shown in Fig. A4a shows the largest uncertainties in the lowermost layer (approx. 1000-800 hPa) which is strongest influenced by the surface fluxes and the smallest uncertainties in the uppermost layer (approx. 200–0 hPa) including the stratosphere. The largest error correlations exist between the layers 1–4, whilst the uncertainties of layer 5 are relatively independent (Fig. A4b). For  $\text{CH}_4$ , the correlation structure is similar (Fig. A4d), but the largest uncertainties are observed in the stratosphere (Fig. A4c).

Also the comparison of SLIM with corresponding TCCON XGAS measurements show good overall agreement (Figs. A5 and A6).

Analysed in the same way as done in the validation study of Reuter et al. (2020), we find  $\text{CO}_2$  biases with a station-to-station standard deviation of 0.57 ppm and an average scatter of 1.14 ppm (Fig. A5a). For  $\text{CH}_4$ , we find biases with a station-to-station standard deviation of 7.5 ppb and an average scatter of 10.6 ppb (Fig. A5b). Especially for  $\text{XCO}_2$ , these values are similar to values found for comparisons of satellite retrieval data products with TCCON (e.g. Reuter et al., 2020).



## Appendix B: Filter variables and bias correction parameters

450 Tables A1 to A12 show the filter settings for the various GOSAT and GOSAT-2 products. Figs. A7 and A8 show the bias correction parameters and their relevance for GOSAT and GOSAT-2.

*Author contributions.* S. Noël adapted the FOCAL method to GOSAT and GOSAT-2, generated the updated FOCAL data products and performed the validation. M. Reuter developed the FOCAL method and provided the XCO<sub>2</sub> and XCH<sub>4</sub> reference databases and the TCCON validation tools. J. Borchardt provided the used python implementation for the SLIM XCO<sub>2</sub> and methane climatology. M. Hilker provided  
455 the original python implementation of FOCAL (OCO-2 version).

A. Di Noia and R. Parker provided the UoL, Y. Yoshida the NIES GOSAT data products.

The following co-authors provided TCCON data: M. Buschmann, N. M. Deutscher, D. G. Feist, D. W. T. Griffith, F. Hase, R. Kivi, C. Liu, Y. Oh, I. Morino, J. Notholt, H. Ohyama, C. Petri, D. F. Pollard, M. Rettinger, C. Roehl, C. Rousogenuous, M. K. Sha, K. Shiomi, K. Strong, R. Sussmann, Y. Té, V. A. Velazco, M. Vrekoussis, T. Warneke.

460 All authors provided support in writing the paper.

*Competing interests.* At least one of the (co-)authors is a member of the editorial board of Atmospheric Measurement Techniques.

*Acknowledgements.* GOSAT and GOSAT-2 spectral data have been provided by JAXA and NIES. CarbonTracker CT2019B and CT-NRT.v2020-1 results were provided by NOAA ESRL, Boulder, Colorado, USA from the website at <http://carbontracker.noaa.gov>. ABSCO cross sections for CO<sub>2</sub> were provided by NASA and the ACOS/OCO-2 team. GMTED2010 topography data were provided by the U.S.  
465 Geological Survey (USGS) and the National Geospatial-Intelligence Agency (NGA). We thank the European Center for Medium Range Weather Forecasts (ECMWF) for providing us with analysed meteorological fields (ERA5 data).

The GOSAT ACOS Level 2 XCO<sub>2</sub> product from the NASA/OCO-2 team has been obtained from [https://oco2.gesdisc.eosdis.nasa.gov/data/GOSAT\\_TANSO\\_Level2/ACOS\\_L2\\_Lite\\_FP9r/](https://oco2.gesdisc.eosdis.nasa.gov/data/GOSAT_TANSO_Level2/ACOS_L2_Lite_FP9r/), <https://doi.org/10.5067/VWSABTO7ZII4>, last access: 16 October 2020. The UoL and SRON GOSAT data products have been obtained from the Copernicus Climate Data Store (<https://cds.climate.copernicus.eu/>, last assess:  
470 15-Oct-2020). GOSAT Level 2 data from NIES have been provided by the GOSAT Data Archive Service (GDAS; <https://data2.gosat.nies.go.jp/>, last access: 17 January 2022).

RJP is funded via the UK National Centre for Earth Observation (NE/N018079/1). This research used the ALICE High Performance Computing Facility at the University of Leicester for the UoL GOSAT retrievals.

The Paris TCCON site has received funding from Sorbonne Université, the French research centre CNRS, the French space agency  
475 CNES, and Région Île-de-France. The Réunion Island station is operated by the Royal Belgian Institute for Space Aeronomy with financial support since 2014 by the EU project ICOS-Inwire and the ministerial decree for ICOS (FR/35/IC1 to FR/35/IC6) and local activities supported by LACy/UMR8105 – Université de La Réunion. The TCCON stations at Rikubetsu, Tsukuba, and Burgos are supported in part by the GOSAT series project. Local support for Burgos is provided by the Energy Development Corporation (EDC, Philippines). The Eureka measurements were made at the Polar Environment Atmospheric Research Laboratory (PEARL) by the Canadian Network for the

480 Detection of Atmospheric Change (CANDAC), primarily supported by the Natural Sciences and Engineering Research Council of Canada,  
Environment and Climate Change Canada, and the Canadian Space Agency. The Anmyeondo TCCON station is funded by the Korea  
Meteorological Administration Research and Development Program “Development of Monitoring and Analysis Techniques for Atmospheric  
Composition in Korea” under grant (KMA2018-00522). The TCCON Nicosia site has received support from the European Unions’ Horizon  
2020 research and innovation programme under grant agreement No. 856612 (EMME-CARE), the Cyprus Government, and by the University  
485 of Bremen. NMD is supported by an Australian Research Council (ARC) Future Fellowship, FT180100327. The Darwin and Wollongong  
TCCON sites have been supported by a series of ARC grants, including DP160100598, DP140100552, DP110103118, DP0879468 and  
LE0668470, and NASA grants NAG5-12247 and NNG05-GD07G.

Large parts of the calculations reported here were performed on HPC facilities of the IUP, University of Bremen, funded under DFG/FUGG  
grant INST 144/379-1 and INST 144/493-1. The work was supported by the Copernicus Atmosphere Monitoring Service (CAMS) via project  
490 CAMS2-52b.

This work has received funding from JAXA (GOSAT and GOSAT-2 support, contracts 19RT000692 and JX-PSPC-527269), EUMETSAT  
(FOCAL-CO2M study, contract EUM/CO/19/4600002372/RL), ESA (GHG-CCI+ project, contract 4000126450/19/I-NB), and the State and  
the University of Bremen.

## References

- 495 Barret, B., Gouzenes, Y., Le Flochmoen, E., and Ferrant, S.: Retrieval of Metop-A/IASI N<sub>2</sub>O Profiles and Validation with NDACC FTIR Data, *Atmosph.*, 12, <https://doi.org/10.3390/atmos12020219>, 2021.
- Benner, D. C., Devi, V. M., Sung, K., Brown, L. R., Miller, C. E., Payne, V. H., Drouin, B. J., Yu, S., Crawford, T. J., Mantz, A. W., Smith, M. A. H., and Gamache, R. R.: Line parameters including temperature dependences of air- and self-broadened line shapes of <sup>12</sup>C<sup>16</sup>O<sub>2</sub>: 2.06- $\mu$ m region, *J. Mol. Spectr.*, 326, 21–47, <https://doi.org/https://doi.org/10.1016/j.jms.2016.02.012>, new Visions of Spectroscopic Databases, Volume I, 2016.
- 500 Bergamaschi, P., Houweling, S., Segers, A., Krol, M., Frankenberg, C., Scheepmaker, R. A., Dlugokencky, E., Wofsy, S. C., Kort, E. A., Sweeney, C., Schuck, T., Brenninkmeijer, C., Chen, H., Beck, V., and Gerbig, C.: Atmospheric CH<sub>4</sub> in the first decade of the 21st century: Inverse modeling analysis using SCIAMACHY satellite retrievals and NOAA surface measurements, *J. Geophys. Res. Atmos.*, 118, 7350–7369, <https://doi.org/https://doi.org/10.1002/jgrd.50480>, 2013.
- 505 Blumenstock, T., Hase, F., Schneider, M., García, O. E., and Sepúlveda, E.: TCCON data from Izana (ES), Release GGG2014.R1, <https://doi.org/10.14291/TCCON.GGG2014.IZANA01.R1>, 2017.
- Boesch, H., Deutscher, N. M., Warneke, T., Byckling, K., Cogan, A. J., Griffith, D. W. T., Notholt, J., Parker, R. J., and Wang, Z.: HDO/H<sub>2</sub>O ratio retrievals from GOSAT, *Atmos. Meas. Tech.*, 6, 599–612, <https://doi.org/10.5194/amt-6-599-2013>, 2013.
- Buchwitz, M., Reuter, M., Schneising-Weigel, O., Aben, I., Wu, L., Hasekamp, O. P., Boesch, H., Noia, A. D., Crevoisier, C., and Armante, R.: Target Requirements and Gap Analysis Document: Greenhouse Gases (CO<sub>2</sub> & CH<sub>4</sub>), Tech. Rep. v3.1 19-02-2021, Copernicus Climate Change Service (C3S, [http://wdc.dlr.de/C3S\\_312b\\_Lot2/Documentation/GHG/TRD-GAD/C3S\\_D312b\\_Lot2.1.0-2020\(GHG\)\\_TRD-GAD\\_v3.1.pdf](http://wdc.dlr.de/C3S_312b_Lot2/Documentation/GHG/TRD-GAD/C3S_D312b_Lot2.1.0-2020(GHG)_TRD-GAD_v3.1.pdf), last access 31 January 2022, 2021.
- 510 Butz, A., Guerlet, S., Hasekamp, O., Schepers, D., Galli, A., Aben, I., Frankenberg, C., Hartmann, J.-M., Tran, H., Kuze, A., Keppel-Aleks, G., Toon, G., Wunch, D., Wennberg, P., Deutscher, N., Griffith, D., Macatangay, R., Messerschmidt, J., Notholt, J., and Warneke, T.: Toward accurate CO<sub>2</sub> and CH<sub>4</sub> observations from GOSAT, *Geophys. Res. Lett.*, 38, <https://doi.org/10.1029/2011GL047888>, 2011.
- 515 Cogan, A. J., Boesch, H., Parker, R. J., Feng, L., Palmer, P. I., Blavier, J.-F. L., Deutscher, N. M., Macatangay, R., Notholt, J., Roehl, C., Warneke, T., and Wunch, D.: Atmospheric carbon dioxide retrieved from the Greenhouse gases Observing SATellite (GOSAT): Comparison with ground-based TCCON observations and GEOS-Chem model calculations, *Journal of Geophysical Research: Atmospheres*, 117, <https://doi.org/10.1029/2012JD018087>, 2012.
- 520 Danielson, J. and Gesch, D.: Global multi-resolution terrain elevation data 2010 (GMTED2010): Open-File Report 2011–1073, Tech. rep., U.S. Geological Survey, <https://doi.org/10.3133/ofr20111073>, 2011.
- De Mazière, M., Sha, M. K., Desmet, F., Hermans, C., Scolas, F., Kumps, N., Metzger, J.-M., Duflot, V., and Cammas, J.-P.: TCCON data from Réunion Island (RE), Release GGG2014.R1, <https://doi.org/10.14291/TCCON.GGG2014.REUNION01.R1>, 2017.
- Deutscher, N. M., Notholt, J., Messerschmidt, J., Weinzierl, C., Warneke, T., Petri, C., and Grupe, P.: TCCON data from Bialystok (PL), Release GGG2014.R2, <https://doi.org/10.14291/TCCON.GGG2014.BIALYSTOK01.R2>, 2019.
- 525 Devi, V. M., Benner, D. C., Sung, K., Brown, L. R., Crawford, T. J., Miller, C. E., Drouin, B. J., Payne, V. H., Yu, S., Smith, M. A. H., Mantz, A. W., and Gamache, R. R.: Line parameters including temperature dependences of self- and air-broadened line shapes of <sup>12</sup>C<sup>16</sup>O<sub>2</sub>: 1.6- $\mu$ m region, *J. Quant. Spectr. Rad. Transf.*, 177, 117–144, <https://doi.org/https://doi.org/10.1016/j.jqsrt.2015.12.020>, XVIIIth Symposium on High Resolution Molecular Spectroscopy (HighRus-2015), Tomsk, Russia, 2016.

- 530 Dubey, M., Lindenmaier, R., Henderson, B., Green, D., Allen, N., Roehl, C., Blavier, J.-F., Butterfield, Z., Love, S., Hamelmann, J., and Wunch, D.: TCCON data from Four Corners (US), Release GGG2014R0, TCCON data archive, hosted by CaltechDATA, <https://doi.org/10.14291/tcon.ggg2014.fourcorners01.R0/1149272>, 2014.
- Dupuy, E., Morino, I., Deutscher, N. M., Yoshida, Y., Uchino, O., Connor, B. J., De Mazière, M., Griffith, D. W. T., Hase, F., Heikkinen, P., Hillyard, P. W., Iraci, L. T., Kawakami, S., Kivi, R., Matsunaga, T., Notholt, J., Petri, C., Podolske, J. R., Pollard, D. F., Rettinger, M., Roehl, C. M., Sherlock, V., Sussmann, R., Toon, G. C., Velazco, V. A., Warneke, T., Wennberg, P. O., Wunch, D., and Yokota, T.: Comparison of XH<sub>2</sub>O Retrieved from GOSAT Short-Wavelength Infrared Spectra with Observations from the TCCON Network, *Rem. Sens.*, 8, <https://doi.org/10.3390/rs8050414>, 2016.
- 535 Feist, D. G., Arnold, S. G., John, N., and Geibel, M. C.: TCCON data from Ascension Island (SH), Release GGG2014R0, TCCON data archive, hosted by CaltechDATA, <https://doi.org/10.14291/tcon.ggg2014.ascension01.R0/1149285>, 2014.
- 540 Frankenberg, C., Wunch, D., Toon, G., Risi, C., Scheepmaker, R., Lee, J.-E., Wennberg, P., and Worden, J.: Water vapor isotopologue retrievals from high-resolution GOSAT shortwave infrared spectra, *Atmos. Meas. Tech.*, 6, 263–274, <https://doi.org/10.5194/amt-6-263-2013>, 2013.
- García, O. E., Schneider, M., Ertl, B., Sepúlveda, E., Borger, C., Diekmann, C., Wiegeler, A., Hase, F., Barthlott, S., Blumenstock, T., Raffalski, U., Gómez-Peláez, A., Steinbacher, M., Ries, L., and de Frutos, A. M.: The MUSICA IASI CH<sub>4</sub> and N<sub>2</sub>O products and their comparison to HIPPO, GAW and NDACC FTIR references, *Atmos. Meas. Tech.*, 11, 4171–4215, <https://doi.org/10.5194/amt-11-4171-2018>, 2018.
- 545 Goo, T.-Y., Oh, Y.-S., and Velazco, V. A.: TCCON data from Anmeyondo (KR), Release GGG2014R0, TCCON data archive, hosted by CaltechDATA, <https://doi.org/10.14291/tcon.ggg2014.anmeyondo01.R0/1149284>, 2014.
- Gordon, I., Rothman, L., Hill, C., Kochanov, R., Tan, Y., Bernath, P., Birk, M., Boudon, V., Campargue, A., Chance, K., Drouin, B., Flaud, J.-M., Gamache, R., Hodges, J., Jacquemart, D., Perevalov, V., Perrin, A., Shine, K., Smith, M.-A., Tennyson, J., Toon, G., Tran, H., Tyuterev, V., Barbe, A., Császár, A., Devi, V., Furtenbacher, T., Harrison, J., Hartmann, J.-M., Jolly, A., Johnson, T., Karman, T., Kleiner, I., Kyuberis, A., Loos, J., Lyulin, O., Massie, S., Mikhailenko, S., Moazzen-Ahmadi, N., Müller, H., Naumenko, O., Nikitin, A., Polyansky, O., Rey, M., Rotger, M., Sharpe, S., Sung, K., Starikova, E., Tashkun, S., Auwera, J. V., Wagner, G., Wilzewski, J., Wcisło, P., Yu, S., and Zak, E.: The HITRAN2016 molecular spectroscopic database, *J. Quant. Spectr. Rad. Transf.*, 203, 3 – 69, <https://doi.org/https://doi.org/10.1016/j.jqsrt.2017.06.038>, hITRAN2016 Special Issue, 2017.
- 555 Gorshelev, V., Serdyuchenko, A., Weber, M., Chehade, W., and Burrows, J. P.: High spectral resolution ozone absorption cross-sections – Part 1: Measurements, data analysis and comparison with previous measurements around 293 K, *Atmos. Meas. Tech.*, 7, 609–624, <https://doi.org/10.5194/amt-7-609-2014>, 2014.
- Griffith, D. W., Deutscher, N. M., Velazco, V. A., Wennberg, P. O., Yavin, Y., Aleks, G. K., Washenfelter, R. a., Toon, G. C., Blavier, J.-F., Murphy, C., Jones, N., Kettlewell, G., Connor, B. J., Macatangay, R., Roehl, C., Ryzek, M., Glowacki, J., Culligan, T., and Bryant, G.: TCCON data from Darwin (AU), Release GGG2014R0, TCCON data archive, hosted by CaltechDATA, <https://doi.org/10.14291/tcon.ggg2014.darwin01.R0/1149290>, 2014a.
- 560 Griffith, D. W., Velazco, V. A., Deutscher, N. M., Murphy, C., Jones, N., Wilson, S., Macatangay, R., Kettlewell, G., Buchholz, R. R., and Rigenbach, M.: TCCON data from Wollongong (AU), Release GGG2014R0, TCCON data archive, hosted by CaltechDATA, <https://doi.org/10.14291/tcon.ggg2014.wollongong01.R0/1149291>, 2014b.
- 565 Hase, F., Blumenstock, T., Dohe, S., Gross, J., and Kiel, M.: TCCON data from Karlsruhe (DE), Release GGG2014R1, TCCON data archive, hosted by CaltechDATA, <https://doi.org/10.14291/tcon.ggg2014.karlsruhe01.R1/1182416>, 2014.

- Hersbach, H., Bell, B., Berrisford, P., Hirahara, S., Horányi, A., Muñoz Sabater, J., Nicolas, J., Peubey, C., Radu, R., Schepers, D., Simmons, A., Soci, C., Abdalla, S., Abellan, X., Balsamo, G., Bechtold, P., Biavati, G., Bidlot, J., Bonavita, M., De Chiara, G., Dahlgren, P., Dee, D., Diamantakis, M., Dragani, R., Flemming, J., Forbes, R., Fuentes, M., Geer, A., Haimberger, L., Healy, S., Hogan, R. J., Hólm, E., Janisková, M., Keeley, S., Laloyaux, P., Lopez, P., Lupu, C., Radnoti, G., de Rosnay, P., Rozum, I., Vamborg, F., Villaume, S., and Thépaut, J.-N.: The ERA5 global reanalysis, *Quart. Jour. R. Met. Soc.*, pp. 1–51, <https://doi.org/10.1002/qj.3803>, 2020.
- Heymann, J., Reuter, M., Hilker, M., Buchwitz, M., Schneising, O., Bovensmann, H., Burrows, J. P., Kuze, A., Suto, H., Deutscher, N. M., Dubey, M. K., Griffith, D. W. T., Hase, F., Kawakami, S., Kivi, R., Morino, I., Petri, C., Roehl, C., Schneider, M., Sherlock, V., Sussmann, R., Velazco, V. A., Warneke, T., and Wunch, D.: Consistent satellite XCO<sub>2</sub> retrievals from SCIAMACHY and GOSAT using the BESD algorithm, *Atmos. Meas. Tech.*, 8, 2961–2980, <https://doi.org/10.5194/amt-8-2961-2015>, 2015.
- Iraci, L. T., Podolske, J., Hillyard, P. W., Roehl, C., Wennberg, P. O., Blavier, J.-F., Allen, N., Wunch, D., Osterman, G. B., and Albertson, R.: TCCON data from Edwards (US), Release GGG2014R1, TCCON data archive, hosted by CaltechDATA, <https://doi.org/10.14291/tcon.ggg2014.edwards01.R1/1255068>, 2016a.
- Iraci, L. T., Podolske, J., Hillyard, P. W., Roehl, C., Wennberg, P. O., Blavier, J.-F., Landeros, J., Allen, N., Wunch, D., Zavaleta, J., Quigley, E., Osterman, G. B., Barrow, E., and Barney, J.: TCCON data from Indianapolis (US), Release GGG2014R1, TCCON data archive, hosted by CaltechDATA, <https://doi.org/10.14291/tcon.ggg2014.indianapolis01.R1/1330094>, 2016b.
- Jacobson, A. R., Schuldt, K. N., Miller, J. B., Oda, T., Tans, P., Arlyn Andrews, Mund, J., Ott, L., Collatz, G. J., Aalto, T., Afshar, S., Aikin, K., Aoki, S., Apadula, F., Baier, B., Bergamaschi, P., Beyersdorf, A., Biraud, S. C., Bollenbacher, A., Bowling, D., Brailsford, G., Abshire, J. B., Chen, G., Huilin Chen, Lukasz Chmura, Sites Climadat, Colomb, A., Conil, S., Cox, A., Cristofanelli, P., Cuevas, E., Curcoll, R., Sloop, C. D., Davis, K., Wekker, S. D., Delmotte, M., DiGangi, J. P., Dlugokencky, E., Ehleringer, J., Elkins, J. W., Emmenegger, L., Fischer, M. L., Forster, G., Frumau, A., Galkowski, M., Gatti, L. V., Gloor, E., Griffis, T., Hammer, S., Haszpra, L., Hatakka, J., Heliasz, M., Hensen, A., Hermanssen, O., Hintsa, E., Holst, J., Jaffe, D., Karion, A., Kawa, S. R., Keeling, R., Keronen, P., Kolari, P., Kominkova, K., Kort, E., Krummel, P., Kubistin, D., Labuschagne, C., Langenfelds, R., Laurent, O., Laurila, T., Lauvaux, T., Law, B., Lee, J., Lehner, I., Leuenberger, M., Levin, I., Levula, J., Lin, J., Lindauer, M., Loh, Z., Lopez, M., Luijkx, I. T., Myhre, C. L., Machida, T., Mammarella, I., Manca, G., Manning, A., Manning, A., Marek, M. V., Marklund, P., Martin, M. Y., Matsueda, H., McKain, K., Meijer, H., Meinhardt, F., Miles, N., Miller, C. E., Mölder, M., Montzka, S., Moore, F., Josep-Anton Morgui, Morimoto, S., Munger, B., Jaroslaw Necki, Newman, S., Nichol, S., Niwa, Y., O'Doherty, S., Mikael Ottosson-Löfvenius, Paplawsky, B., Peischl, J., Peltola, O., Jean-Marc Pichon, Piper, S., Plass-Dömler, C., Ramonet, M., Reyes-Sanchez, E., Richardson, S., Riris, H., Ryerson, T., Saito, K., Sargent, M., Sasakawa, M., Sawa, Y., Say, D., Scheeren, B., Schmidt, M., Schmidt, A., Schumacher, M., Shepson, P., Shook, M., Stanley, K., Steinbacher, M., Stephens, B., Sweeney, C., Thoning, K., Torn, M., Turnbull, J., Tørseth, K., Bulk, P. V. D., Dinter, D. V., Vermeulen, A., Viner, B., Vitkova, G., Walker, S., Weyrauch, D., Wofsy, S., Worthy, D., Dickon Young, and Miroslaw Zimnoch: CarbonTracker CT2019B, <https://doi.org/10.25925/20201008>, 2020.
- Kawakami, S., Ohyama, H., Arai, K., Okumura, H., Taura, C., Fukamachi, T., and Sakashita, M.: TCCON data from Saga (JP), Release GGG2014R0, TCCON data archive, hosted by CaltechDATA, <https://doi.org/10.14291/tcon.ggg2014.saga01.R0/1149283>, 2014.
- Kivi, R., Heikkinen, P., and Kyrö, E.: TCCON data from Sodankyla (FI), Release GGG2014R0, TCCON data archive, hosted by CaltechDATA, <https://doi.org/10.14291/tcon.ggg2014.sodankyla01.R0/1149280>, 2014.
- Kuze, A., Suto, H., Nakajima, M., and Hamazaki, T.: Thermal and near infrared sensor for carbon observation Fourier-transform spectrometer on the Greenhouse Gases Observing Satellite for greenhouse gases monitoring, *Appl. Optics*, 48, 6716–6733, <https://doi.org/10.1364/AO.48.006716>, 2009.

- Kuze, A., Suto, H., Shiomi, K., Kawakami, S., Tanaka, M., Ueda, Y., Deguchi, A., Yoshida, J., Yamamoto, Y., Kataoka, F., Taylor, T. E., and Buijs, H. L.: Update on GOSAT TANSO-FTS performance, operations, and data products after more than 6 years in space, *Atmos. Meas. Tech.*, 9, 2445–2461, <https://doi.org/10.5194/amt-9-2445-2016>, 2016.
- Liu, C., Wang, W., Sun, Y., and , : TCCON data from Hefei (PRC), Release GGG2014.R0, 610 <https://doi.org/10.14291/TCCON.GGG2014.HEFEI01.R0>, 2018.
- Morino, I., Yokozeki, N., Matzuzaki, T., and Horikawa, M.: TCCON data from Rikubetsu (JP), Release GGG2014R2, TCCON data archive, hosted by CaltechDATA, <https://doi.org/10.14291/tcon.ggg2014.rikubetsu01.R2>, 2017.
- Morino, I., Matsuzaki, T., and Horikawa, M.: TCCON data from Tsukuba (JP), 125HR, Release GGG2014.R2, <https://doi.org/10.14291/TCCON.GGG2014.TSUKUBA02.R2>, 2018a.
- 615 Morino, I., Velazco, V. A., Akihiro, H., Osamu, U., and Griffith, D. W. T.: TCCON data from Burgos, Ilocos Norte (PH), Release GGG2014.R0, TCCON data archive, hosted by CaltechDATA, <https://doi.org/10.14291/tcon.ggg2014.burgos01.R0>, 2018b.
- Noël, S., Reuter, M., Buchwitz, M., Borchardt, J., Hilker, M., Bovensmann, H., Burrows, J. P., Di Noia, A., Suto, H., Yoshida, Y., Buschmann, M., Deutscher, N. M., Feist, D. G., Griffith, D. W. T., Hase, F., Kivi, R., Morino, I., Notholt, J., Ohyama, H., Petri, C., Podolske, J. R., Pollard, D. F., Sha, M. K., Shiomi, K., Sussmann, R., Té, Y., Velazco, V. A., and Warneke, T.: XCO<sub>2</sub> retrieval for GOSAT and GOSAT-2 620 based on the FOCAL algorithm, *Atmos. Meas. Tech.*, 14, 3837–3869, <https://doi.org/10.5194/amt-14-3837-2021>, 2021.
- Notholt, J., Petri, C., Warneke, T., Deutscher, N. M., Palm, M., Buschmann, M., Weinzierl, C., Macatangay, R. C., and Grupe, P.: TCCON data from Bremen (DE), Release GGG2014.R1, <https://doi.org/10.14291/TCCON.GGG2014.BREMEN01.R1>, 2019a.
- Notholt, J., Schrems, O., Warneke, T., Deutscher, N., Weinzierl, C., Palm, M., Buschmann, M., and Engineers, A.-P. S.: TCCON data from Ny Ålesund, Spitsbergen (NO), Release GGG2014.R1, <https://doi.org/10.14291/tcon.ggg2014.nyalesund01.R1>, 2019b.
- 625 Parker, R., Boesch, H., Cogan, A., Fraser, A., Feng, L., Palmer, P. I., Messerschmidt, J., Deutscher, N., Griffith, D. W. T., Notholt, J., Wennberg, P. O., and Wunch, D.: Methane observations from the Greenhouse Gases Observing SATellite: Comparison to ground-based TCCON data and model calculations, *Geophys. Res. Lett.*, 38, <https://doi.org/https://doi.org/10.1029/2011GL047871>, 2011.
- Parker, R. J., Webb, A., Boesch, H., Somkuti, P., Barrio Guillo, R., Di Noia, A., Kalaitzi, N., Anand, J. S., Bergamaschi, P., Chevallier, F., Palmer, P. I., Feng, L., Deutscher, N. M., Feist, D. G., Griffith, D. W. T., Hase, F., Kivi, R., Morino, I., Notholt, J., Oh, Y.-S., Ohyama, H., 630 Petri, C., Pollard, D. F., Roehl, C., Sha, M. K., Shiomi, K., Strong, K., Sussmann, R., Té, Y., Velazco, V. A., Warneke, T., Wennberg, P. O., and Wunch, D.: A decade of GOSAT Proxy satellite CH<sub>4</sub> observations, *Earth Syst. Sci. Data*, 12, 3383–3412, <https://doi.org/10.5194/essd-12-3383-2020>, 2020.
- Petri, C., Vrekoussis, M., Rousogenous, C., Warneke, T., Sciare, J., and Notholt, J.: TCCON data from Nicosia, Cyprus (CY), Release GGG2014.R0, <https://doi.org/10.14291/TCCON.GGG2014.NICOSIA01.R0>, 2020.
- 635 Pollard, D. F., Robinson, J., and Shiona, H.: TCCON data from Lauder (NZ), Release GGG2014.R0, <https://doi.org/10.14291/TCCON.GGG2014.LAUDER03.R0>, 2019.
- Reuter, M., Buchwitz, M., Schneising, O., Noël, S., Bovensmann, H., and Burrows, J. P.: A Fast Atmospheric Trace Gas Retrieval for Hyperspectral Instruments Approximating Multiple Scattering – Part 2: Application to XCO<sub>2</sub> Retrievals from OCO-2, *Rem. Sens.*, 9, 1102, <https://doi.org/10.3390/rs9111102>, 2017a.
- 640 Reuter, M., Buchwitz, M., Schneising, O., Noël, S., Rozanov, V., Bovensmann, H., and Burrows, J. P.: A Fast Atmospheric Trace Gas Retrieval for Hyperspectral Instruments Approximating Multiple Scattering – Part 1: Radiative Transfer and a Potential OCO-2 XCO<sub>2</sub> Retrieval Setup, *Rem. Sens.*, 9, 1159, <https://doi.org/10.3390/rs9111159>, 2017b.

- Reuter, M., Buchwitz, M., and Schneising-Weigel, O.: ProductQuality Assessment Report (PQAR) – ANNEX D for products XCO<sub>2</sub>\_EMMA, XCH<sub>4</sub>\_EMMA, XCO<sub>2</sub>\_OBS4MIPS, XCH<sub>4</sub>\_OBS4MIPS (v4.1, 2003–2018), Tech. Rep. version 3.1, 03-11-2019, Copernicus Climate Change Service (C3S, [http://www.iup.uni-bremen.de/carbon\\_ghg/docs/C3S/CDR3\\_2003-2018/PQAR/C3S\\_D312b\\_Lot2.2.3.2-v1.0\\_PQAR-GHG\\_ANNEX-D\\_v3.1.pdf](http://www.iup.uni-bremen.de/carbon_ghg/docs/C3S/CDR3_2003-2018/PQAR/C3S_D312b_Lot2.2.3.2-v1.0_PQAR-GHG_ANNEX-D_v3.1.pdf), last access:10 January 2020, 2019.
- Reuter, M., Buchwitz, M., Schneising, O., Noël, S., Bovensmann, H., Burrows, J. P., Boesch, H., Di Noia, A., Anand, J., Parker, R. J., Somkuti, P., Wu, L., Hasekamp, O. P., Aben, I., Kuze, A., Suto, H., Shiomi, K., Yoshida, Y., Morino, I., Crisp, D., O'Dell, C. W., Notholt, J., Petri, C., Warneke, T., Velazco, V. A., Deutscher, N. M., Griffith, D. W. T., Kivi, R., Pollard, D. F., Hase, F., Sussmann, R., Té, Y. V., Strong, K., Roche, S., Sha, M. K., De Mazière, M., Feist, D. G., Iraci, L. T., Roehl, C. M., Retscher, C., and Schepers, D.: Ensemble-based satellite-derived carbon dioxide and methane column-averaged dry-air mole fraction data sets (2003–2018) for carbon and climate applications, *Atmos. Meas. Tech.*, 13, 789–819, <https://doi.org/10.5194/amt-13-789-2020>, 2020.
- Ricaud, P., Attié, J.-L., Teyssèdre, H., El Amraoui, L., Peuch, V.-H., Matricardi, M., and Schluessel, P.: Equatorial total column of nitrous oxide as measured by IASI on MetOp-A: implications for transport processes, *Atmos. Chem. Phys.*, 9, 3947–3956, <https://doi.org/10.5194/acp-9-3947-2009>, 2009.
- Schepers, D., Guerlet, S., Butz, A., Landgraf, J., Frankenberg, C., Hasekamp, O., Blavier, J.-F., Deutscher, N. M., Griffith, D. W. T., Hase, F., Kyro, E., Morino, I., Sherlock, V., Sussmann, R., and Aben, I.: Methane retrievals from Greenhouse Gases Observing Satellite (GOSAT) shortwave infrared measurements: Performance comparison of proxy and physics retrieval algorithms, *J. Geophys. Res. Atmos.*, 117, <https://doi.org/https://doi.org/10.1029/2012JD017549>, 2012.
- Serdyuchenko, A., Gorshelev, V., Weber, M., Chehade, W., and Burrows, J. P.: High spectral resolution ozone absorption cross-sections – Part 2: Temperature dependence, *Atmos. Meas. Tech.*, 7, 625–636, <https://doi.org/10.5194/amt-7-625-2014>, 2014.
- Sherlock, V., Connor, B. J., Robinson, J., Shiona, H., Smale, D., and Pollard, D.: TCCON data from Lauder (NZ), 120HR, Release GGG2014R0, TCCON data archive, hosted by CaltechDATA, <https://doi.org/10.14291/tcon.ggg2014.lauder01.R0/1149293>, 2014a.
- Sherlock, V., Connor, B. J., Robinson, J., Shiona, H., Smale, D., and Pollard, D.: TCCON data from Lauder (NZ), 125HR, Release GGG2014R0, TCCON data archive, hosted by CaltechDATA, <https://doi.org/10.14291/tcon.ggg2014.lauder02.R0/1149298>, 2014b.
- Strong, K., Roche, S., Franklin, J. E., Mendonca, J., Lutsch, E., Weaver, D., Fogal, P. F., Drummond, J. R., Batchelor, R., and Lindenmaier, R.: TCCON data from Eureka (CA), Release GGG2014.R3, <https://doi.org/10.14291/TCCON.GGG2014.EUREKA01.R3>, 2019.
- Sussmann, R. and Rettinger, M.: TCCON data from Garmisch (DE), Release GGG2014.R2, <https://doi.org/10.14291/TCCON.GGG2014.GARMISCH01.R2>, 2018a.
- Sussmann, R. and Rettinger, M.: TCCON data from Zugspitze (DE), Release GGG2014R1, TCCON data archive, hosted by CaltechDATA, <https://doi.org/10.14291/tcon.ggg2014.zugspitze01.R1>, 2018b.
- Suto, H., Kataoka, F., Kikuchi, N., Knuteson, R. O., Butz, A., Haun, M., Buijs, H., Shiomi, K., Imai, H., and Kuze, A.: Thermal and near-infrared sensor for carbon observation Fourier transform spectrometer-2 (TANSO-FTS-2) on the Greenhouse gases Observing SATellite-2 (GOSAT-2) during its first year in orbit, *Atmos. Meas. Tech.*, 14, 2013–2039, <https://doi.org/10.5194/amt-14-2013-2021>, 2021.
- Taylor, T. E., O'Dell, C. W., Crisp, D., Kuze, A., Lindqvist, H., Wennberg, P. O., Chatterjee, A., Gunson, M., Eldering, A., Fisher, B., Kiel, M., Nelson, R. R., Merrelli, A., Osterman, G., Chevallier, F., Palmer, P. I., Feng, L., Deutscher, N. M., Dubey, M. K., Feist, D. G., García, O. E., Griffith, D. W. T., Hase, F., Iraci, L. T., Kivi, R., Liu, C., De Mazière, M., Morino, I., Notholt, J., Oh, Y.-S., Ohyama, H., Pollard, D. F., Rettinger, M., Schneider, M., Roehl, C. M., Sha, M. K., Shiomi, K., Strong, K., Sussmann, R., Té, Y., Velazco, V. A., Vrekoussis, M., Warneke, T., and Wunch, D.: An 11-year record of XCO<sub>2</sub> estimates derived from GOSAT measurements using the NASA ACOS version 9 retrieval algorithm, *Earth Syst. Sci. Data*, 14, 325–360, <https://doi.org/10.5194/essd-14-325-2022>, 2022.



- Te, Y., Jeseck, P., and Janssen, C.: TCCON data from Paris (FR), Release GGG2014R0, TCCON data archive, hosted by CaltechDATA, <https://doi.org/10.14291/tcon.ggg2014.paris01.R0/1149279>, 2014.
- Warneke, T., Messerschmidt, J., Notholt, J., Weinzierl, C., Deutscher, N. M., Petri, C., and Grupe, P.: TCCON data from Orléans (FR), Release GGG2014.R1, <https://doi.org/10.14291/TCCON.GGG2014.ORLEANS01.R1>, 2019.
- 685 Wennberg, P. O., Wunch, D., Roehl, C. M., Blavier, J.-F., Toon, G. C., and Allen, N. T.: TCCON data from Caltech (US), Release GGG2014.R1, <https://doi.org/10.14291/TCCON.GGG2014.PASADENA01.R1/1182415>, 2015.
- Wennberg, P. O., Wunch, D., Roehl, C., Blavier, J.-F., Toon, G. C., Allen, N., Dowell, P., Teske, K., Martin, C., and Martin, J.: TCCON data from Lamont (US), Release GGG2014R1, TCCON data archive, hosted by CaltechDATA, <https://doi.org/10.14291/tcon.ggg2014.lamont01.R1/1255070>, 2016.
- 690 Wennberg, P. O., Roehl, C. M., Wunch, D., Toon, G. C., Blavier, J.-F., Washenfelder, R., Keppel-Aleks, G., Allen, N. T., and Ayers, J.: TCCON data from Park Falls (US), Release GGG2014.R1, <https://doi.org/10.14291/TCCON.GGG2014.PARKFALLS01.R1>, 2017.
- Wu, L., Buchwitz, M., Aben, I., Wu, L., and Hasekamp, O. P.: Algorithm Theoretical Basis Document (ATBD) – ANNEX C for product CH<sub>4</sub>\_GOS\_SRPR (v2.3.9, 2009-mid2020), Tech. Rep. v5.0, 18-12-2021, Copernicus Climate Change Service (C3S, [https://www.iup.uni-bremen.de/carbon\\_ghg/docs/C3S/CDR5\\_2003-mid2020/C3S\\_D312b\\_Lot2.1.3.2-v3.0\\_ATBD-GHG\\_ANNEX-C\\_v5.0.pdf](https://www.iup.uni-bremen.de/carbon_ghg/docs/C3S/CDR5_2003-mid2020/C3S_D312b_Lot2.1.3.2-v3.0_ATBD-GHG_ANNEX-C_v5.0.pdf), last access 31 January 2022, 2021.
- 695 Wunch, D., Toon, G. C., Wennberg, P. O., Wofsy, S. C., Stephens, B. B., Fischer, M. L., Uchino, O., Abshire, J. B., Bernath, P., Biraud, S. C., Blavier, J. F. L., Boone, C., Bowman, K. P., Browell, E. V., Campos, T., Connor, B. J., Daube, B. C., Deutscher, N. M., Diao, M., Elkins, J. W., Gerbig, C., Gottlieb, E., Griffith, D. W. T., Hurst, D. F., Jiménez, R., Keppel-Aleks, G., Kort, E. A., Macatangay, R., Machida, T., Matsueda, H., Moore, F., Morino, I., Park, S., Robinson, J., Roehl, C. M., Sawa, Y., Sherlock, V., Sweeney, C., Tanaka,
- 700 T., and Zondlo, M. A.: Calibration of the Total Carbon Column Observing Network using aircraft profile data, *Atmos. Meas. Tech.*, 3, 1351–1362, <https://doi.org/10.5194/amt-3-1351-2010>, 2010.
- Wunch, D., Toon, G. C., Blavier, J.-F. L., Washenfelder, R. A., Notholt, J., Connor, B. J., Griffith, D. W. T., Sherlock, V., and Wennberg, P. O.: The Total Carbon Column Observing Network, *Phil. Trans. R. Soc. A*, 369, 2087–2112, <https://doi.org/10.1098/rsta.2010.0240>, 2011.
- Wunch, D., Mendonca, J., Colebatch, O., Allen, N., Blavier, J.-F. L., Roche, S., Hedelius, J. K., Neufeld, G., Springett, S., Worthy, D.
- 705 E. J., Kessler, R., and Strong, K.: TCCON data from East Trout Lake (CA), Release GGG2014R1, TCCON data archive, hosted by CaltechDATA, <https://doi.org/10.14291/tcon.ggg2014.easttroutlake01.R1>, 2017.
- Yoshida, Y., Kikuchi, N., Morino, I., Uchino, O., Oshchepkov, S., Bril, A., Saeki, T., Schutgens, N., Toon, G. C., Wunch, D., and et al.: Improvement of the retrieval algorithm for GOSAT SWIR XCO<sub>2</sub> and XCH<sub>4</sub> and their validation using TCCON data, *Atmos. Meas. Tech.*, 6, 1533–1547, <https://doi.org/10.5194/amt-6-1533-2013>, 2013.

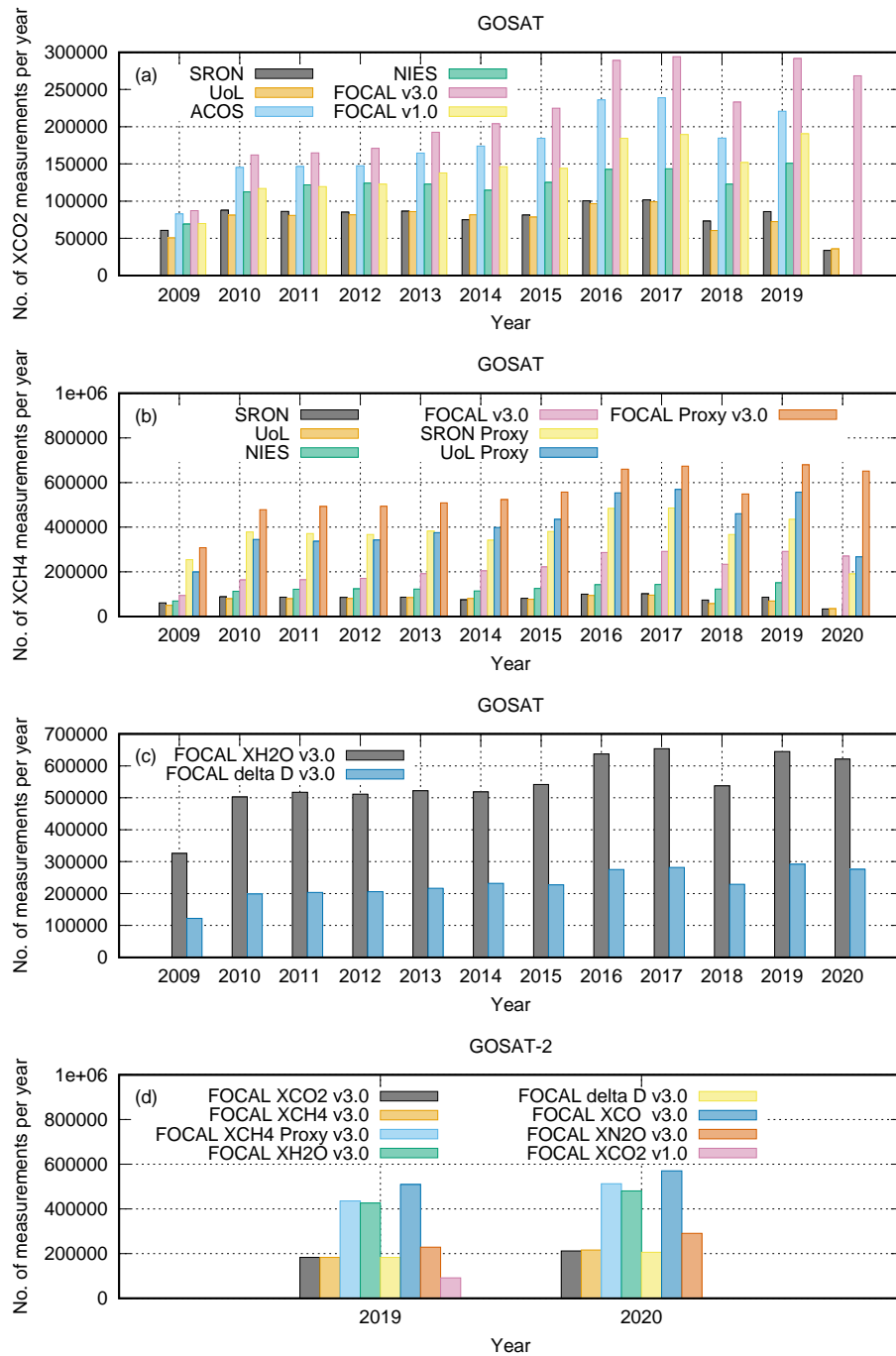


**Figure 1.** Number of GOSAT and GOSAT-2 data for different products as function of time (see Tab. 6 for details on version numbers). (a) GOSAT XCO<sub>2</sub>. (b) GOSAT XCH<sub>4</sub>. (c) GOSAT FOCAL XH<sub>2</sub>O and  $\delta$ D. (d) GOSAT-2 FOCAL products

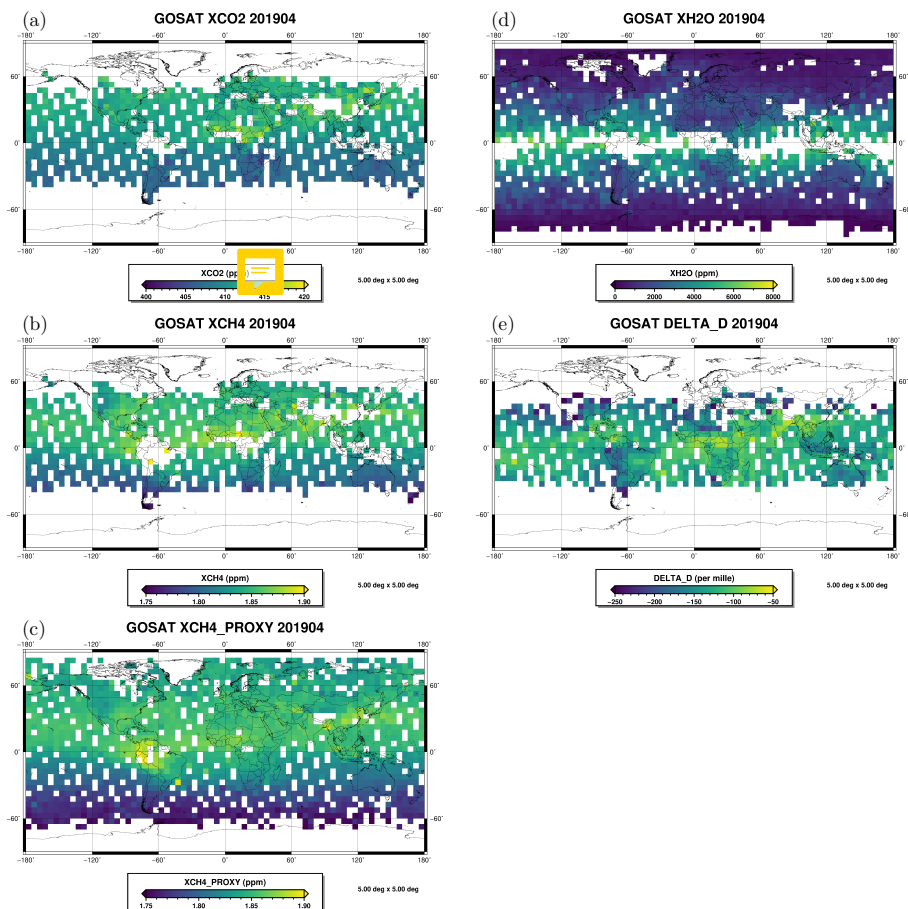


**Figure 2.** Maps of gridded GOSAT data for April 2019: (a) XCO<sub>2</sub>. (b) XCH<sub>4</sub> full physics product. (c) XCH<sub>4</sub> proxy product. (d) XH<sub>2</sub>O. (e)  $\delta$ D.

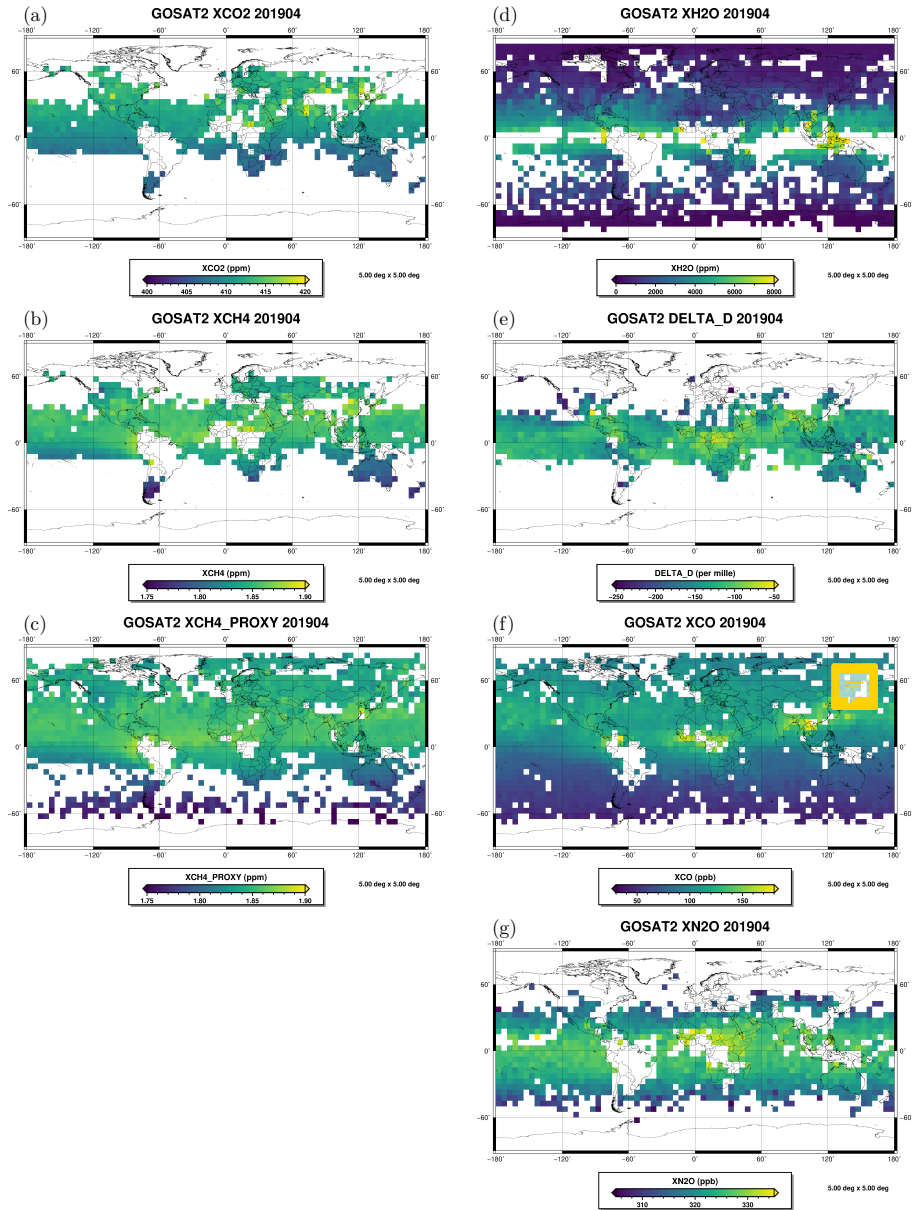


**Figure 3.** Maps of gridded GOSAT-2 data for April 2019: (a) XCO<sub>2</sub>. (b) XCH<sub>4</sub> full physics product. (c) XCH<sub>4</sub> proxy product. (d) XH<sub>2</sub>O. (e) δD. (f) XCO. (g) XN<sub>2</sub>O.

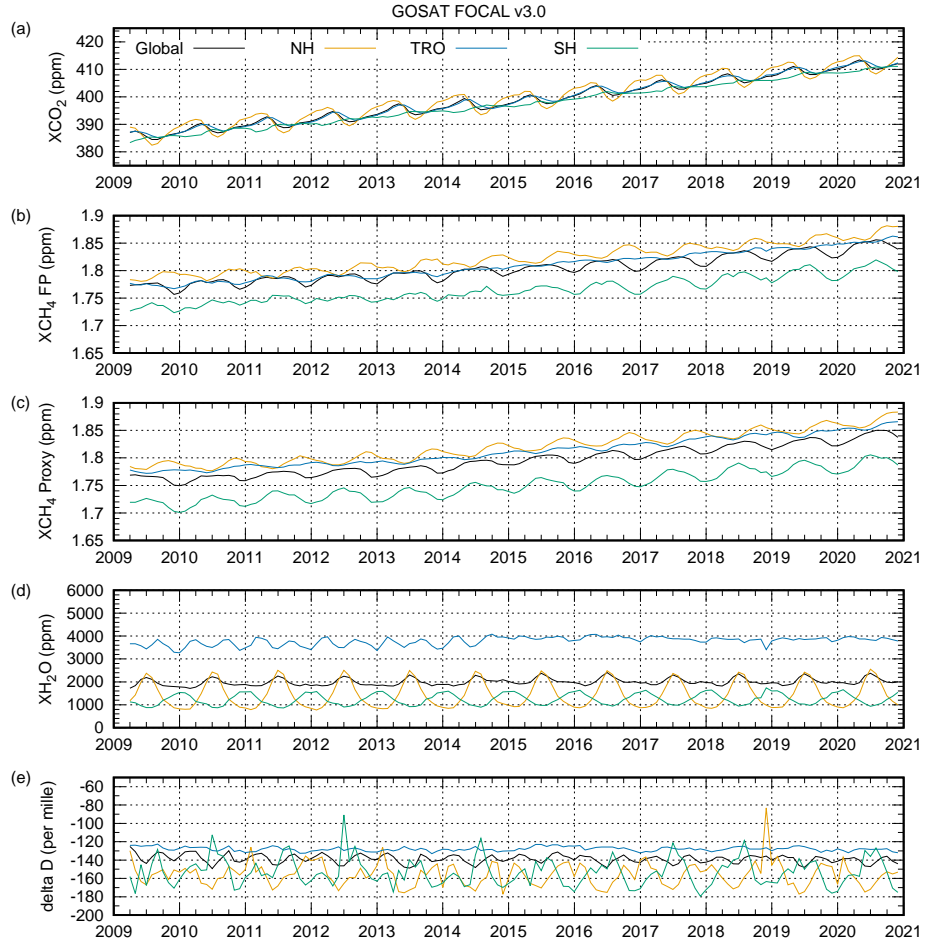


**Figure 4.** GOSAT FOCAL v3.0 time series. NH = Northern hemisphere ( $> 25^\circ N$ ). TRO = Tropics ( $25^\circ S - 25^\circ N$ ). SH = Southern hemisphere ( $< 25^\circ S$ ). (a)  $XCO_2$ . (b)  $XCH_4$  full physics product. (c)  $XCH_4$  proxy product. (d)  $XH_2O$ . (e)  $\delta D$ .

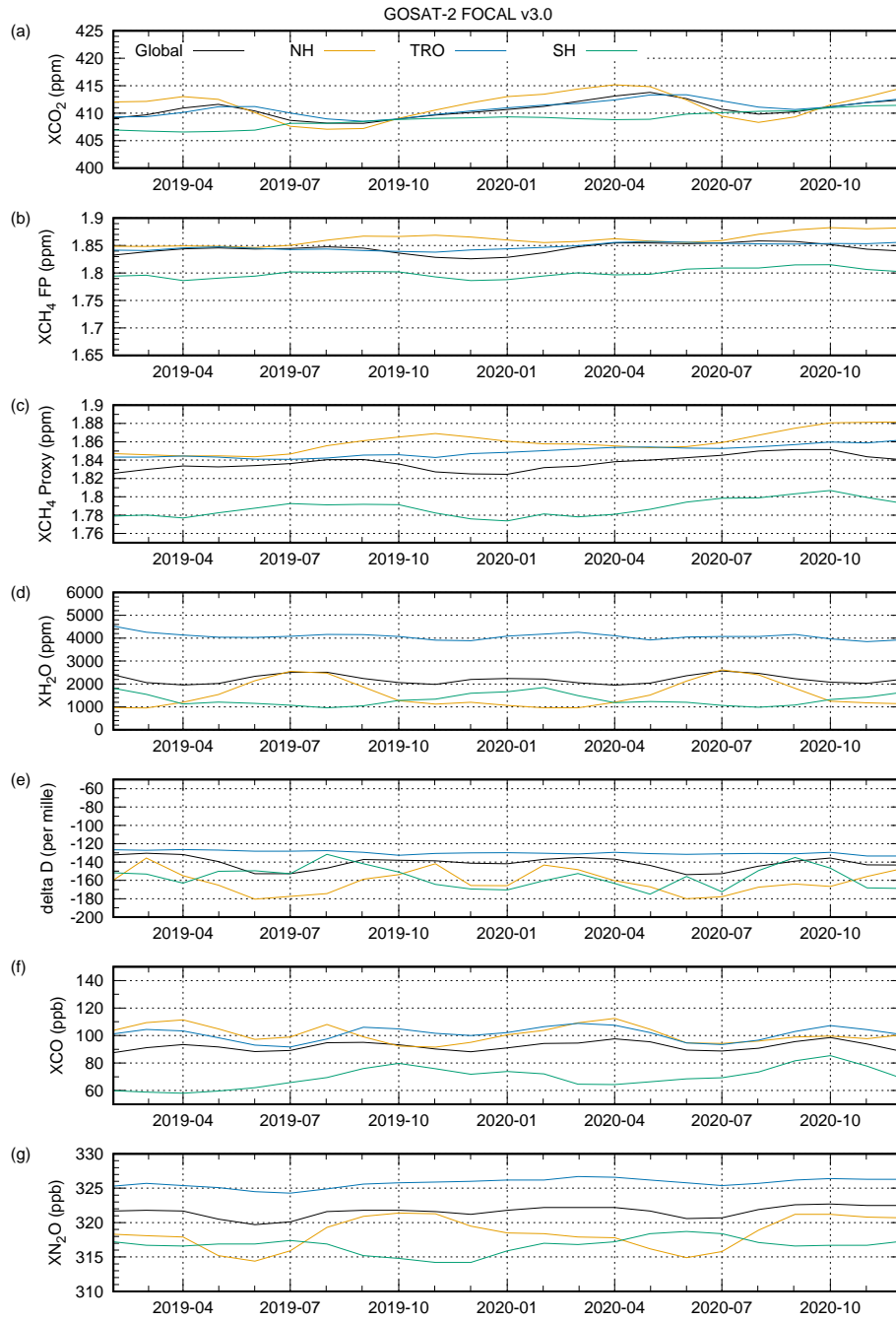


**Figure 2** GOSAT-2 time series. NH = Northern hemisphere ( $> 25^\circ N$ ). TRO = Tropics ( $25^\circ S - 25^\circ N$ ). SH = Southern hemisphere ( $< 25^\circ S$ ). (a)  $XCO_2$ . (b)  $XCH_4$  full physics product. (c)  $XCH_4$  proxy product. (d)  $XH_2O$ . (e)  $\delta D$ . (f)  $XCO$ . (g)  $XN_2O$ .

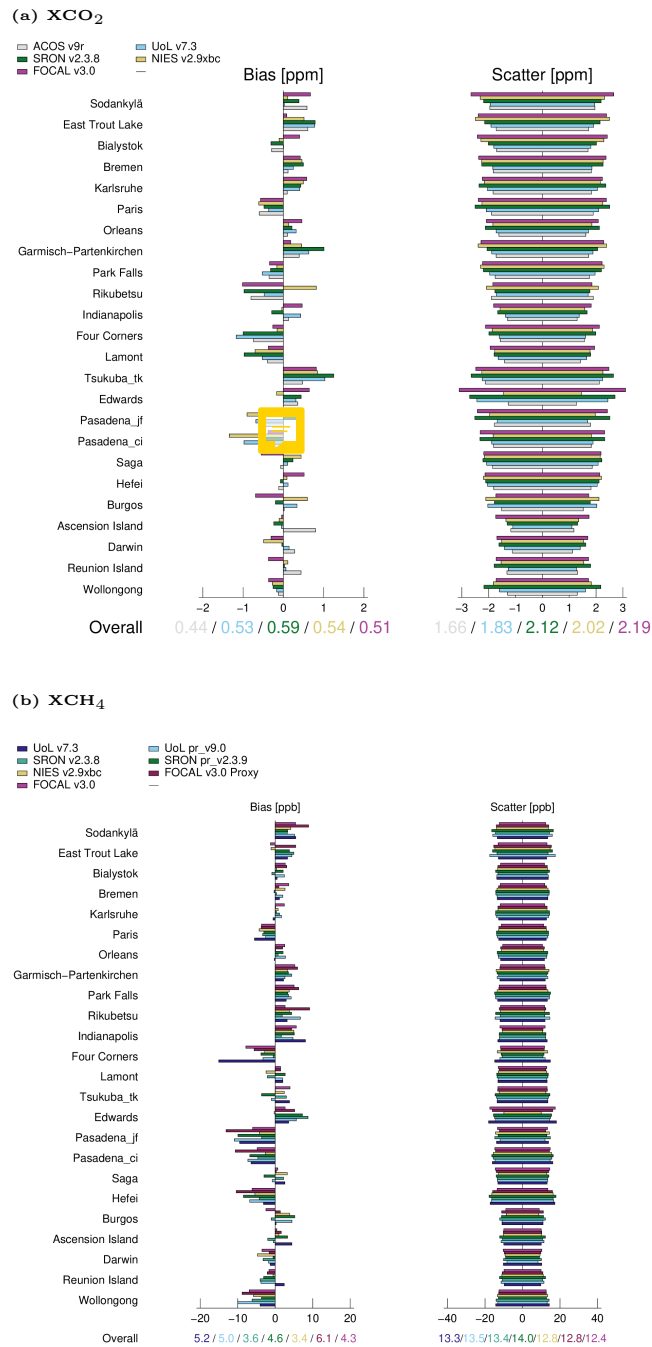
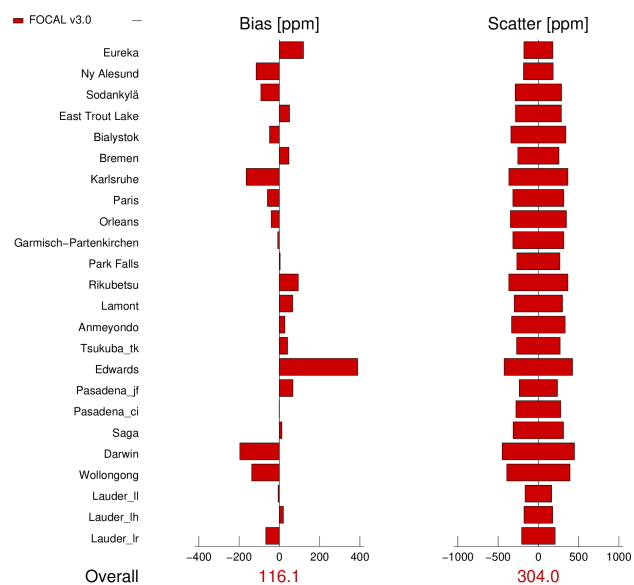


**Figure 6.** Overview of comparison results between different GOSAT products and TCCON data: Scatter and bias for different TCCON stations. Note that the mean station bias has been subtracted to better illustrate the local station differences. (c)  $\text{XH}_2\text{O}$ . (d)  $\delta\text{D}$ .



(a)  $\text{XH}_2\text{O}$



(b)  $\delta\text{D}$

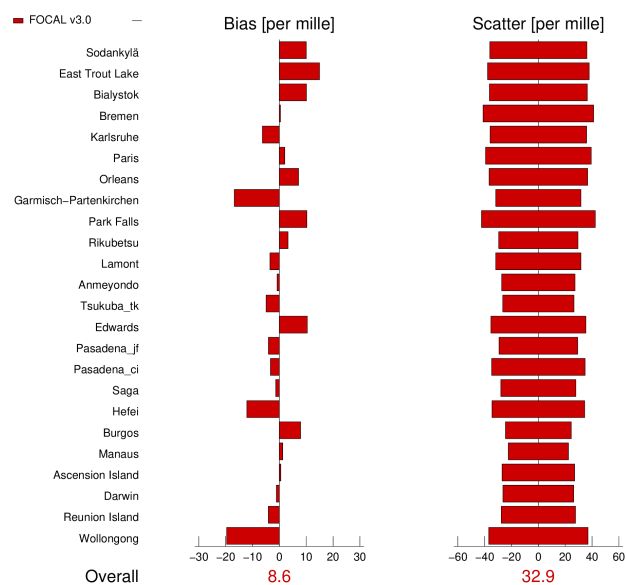
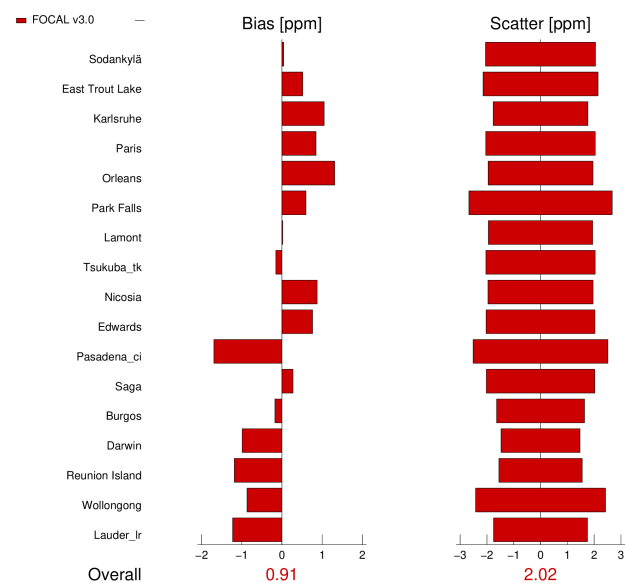
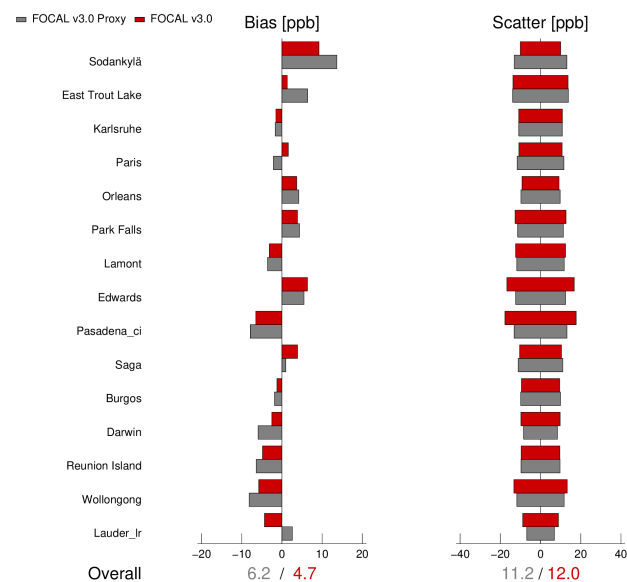


Figure 7. As Figure 6, but for: (a)  $\text{XH}_2\text{O}$ . (b)  $\delta\text{D}$ .

(a)  $\text{XCO}_2$

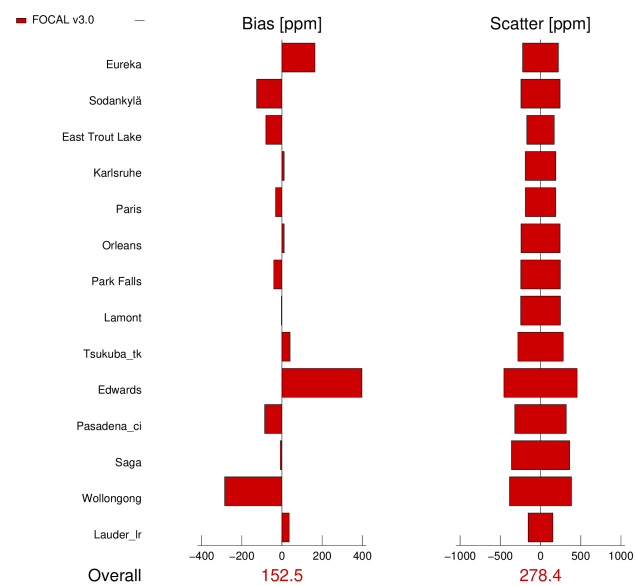


(b)  $\text{XCH}_4$



**Figure 8.** Overview of comparison results between GOSAT-2 FOCAL products and TCCON data: Scatter and bias for different TCCON stations. Note that the mean station bias has been subtracted to better illustrate the local station differences. (a)  $\text{XCO}_2$ . (b)  $\text{XCH}_4$  (full physics and proxy products).

(a)  $\text{XH}_2\text{O}$



(b)  $\delta\text{D}$

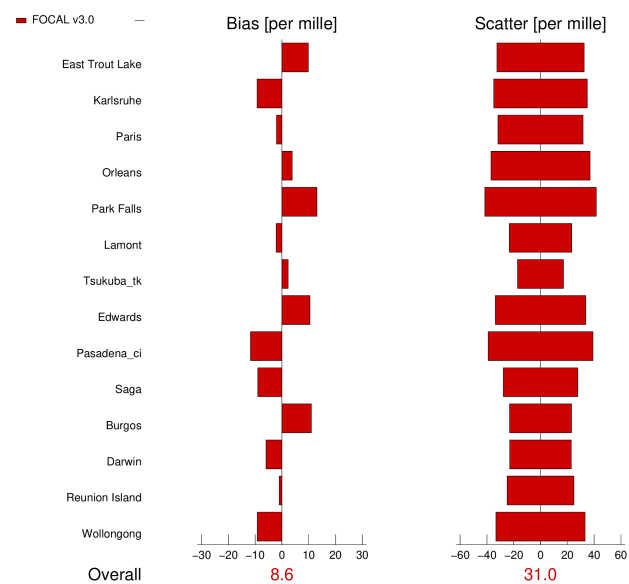
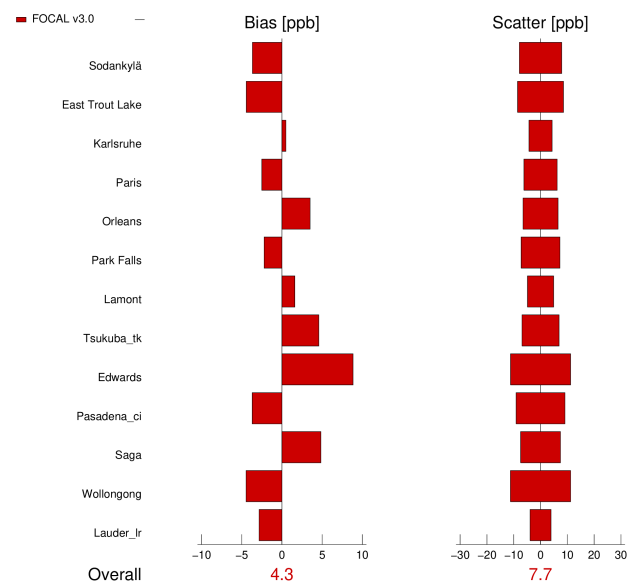


**Figure 9.** As Fig. 8, but for: (a)  $\text{XH}_2\text{O}$ . (b)  $\delta\text{D}$ .

**(a) XCO**



**(b) XN<sub>2</sub>O**

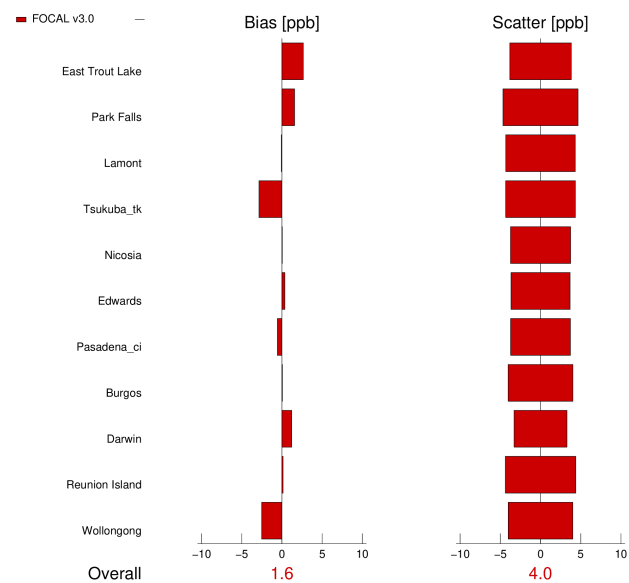


**Figure 10.** As Fig. 8, but for: (a) XCO. (b) XN<sub>2</sub>O.

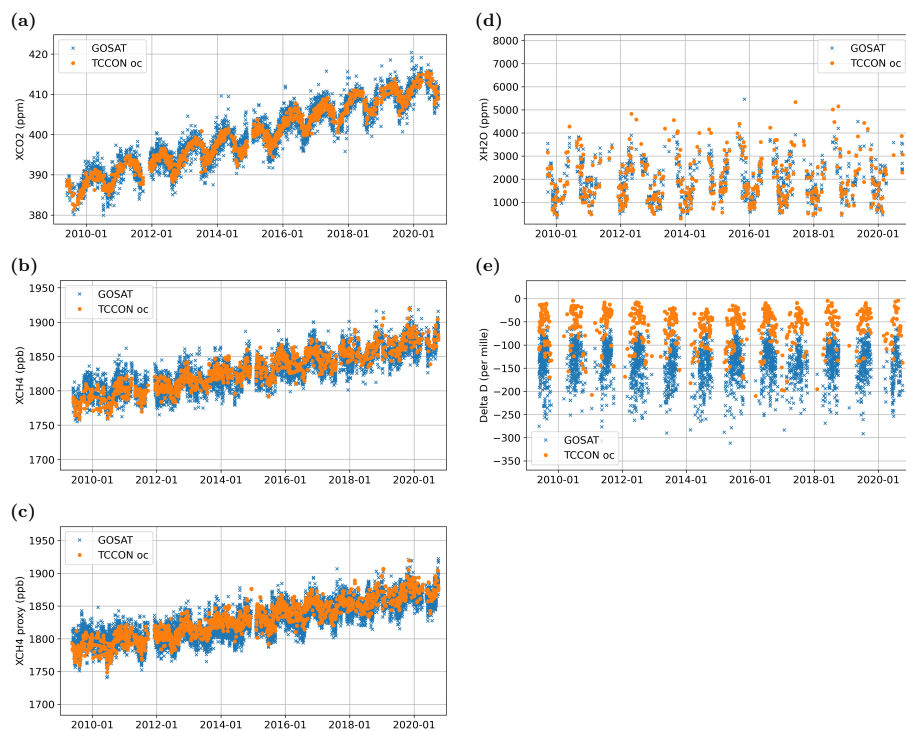


**Figure 11.** Example time series of TCCON and GOSAT FOCAL data at Lamont (station code oc). (a)  $XCO_2$ . (b)  $XCH_4$  full physics product. (c)  $XCH_4$  proxy product. (d)  $XH_2O$ . (e)  $\delta D$ .

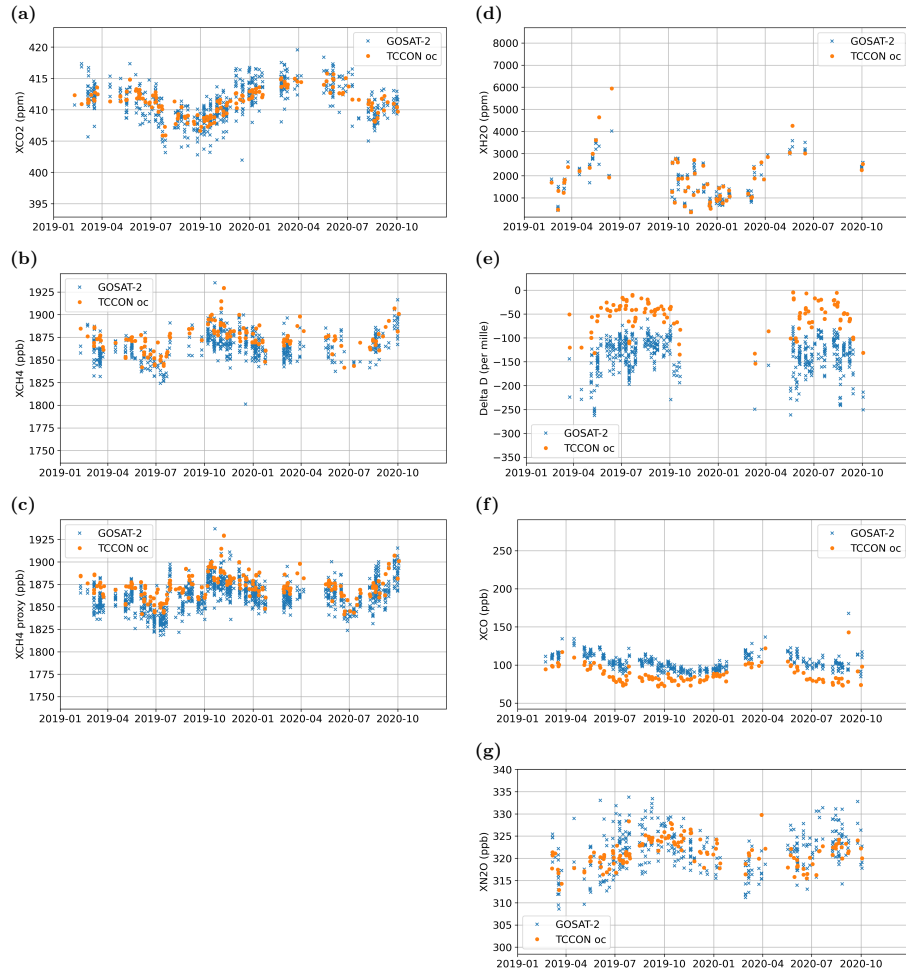


**Figure 12** Example time series of TCCON and GOSAT-2 FOCAL data at Lamont (station code oc). (a)  $\text{XCO}_2$ . (b)  $\text{XCH}_4$  full physics product. (c)  $\text{XCH}_4$  proxy product. (d)  $\text{XH}_2\text{O}$ . (e)  $\delta\text{D}$ . (f)  $\text{XCO}$ . (g)  $\text{XN}_2\text{O}$ .

**Table 1.** TCCON stations used in this study (update of similar table in Noël et al. (2021)).

Site	Lon. (deg)	Lat. (deg)	Elev. (km)	Reference(s)
Anmeyondo (KR)	126.33	36.54	0.03	Goo et al. (2014)
Ascension Island (SH)	-14.33	-7.92	0.01	Feist et al. (2014)
Bialystok (PL)	23.03	53.23	0.18	Deutscher et al. (2019)
Bremen (DE)	8.85	53.10	0.04	Notholt et al. (2019a)
Burgos (PH)	120.65	18.53	0.04	Morino et al. (2018b)
Darwin (AU)	130.89	-12.42	0.03	Griffith et al. (2014a)
Edwards (US)	-117.88	34.96	0.70	Iraci et al. (2016a)
East Trout Lake (CA)	-104.99	54.35	0.50	Wunch et al. (2017)
Eureka (CA)	-86.42	80.05	0.61	Strong et al. (2019)
Four Corners (US)	-108.48	36.80	1.64	Dubey et al. (2014)
Garmisch-Partenkirchen (DE)	11.06	47.48	0.74	Sussmann and Rettinger (2018a)
Hefei (CN)	117.17	31.90	0.04	Liu et al. (2018)
Indianapolis (US)	-86.00	39.86	0.27	Iraci et al. (2016b)
Izaña (ES)	-16.50	28.30	2.37	Blumenstock et al. (2017)
Karlsruhe (DE)	8.43	49.10	0.11	Hase et al. (2014)
Lamont (US)	-97.49	36.60	0.32	Wennberg et al. (2016)
Lauder (NZ)	169.68	-45.04	0.37	Sherlock et al. (2014a, b)
				Pollard et al. (2019)
Nicosia (CY)	33.38	35.14	0.19	Petri et al. (2020)
Ny Ålesund (NO)	11.90	78.90	0.02	Notholt et al. (2019b)
Orleans (FR)	2.11	47.97	0.13	Warneke et al. (2019)
Paris (FR)	2.36	48.85	0.06	Te et al. (2014)
Park Falls (US)	-90.27	45.95	0.44	Wennberg et al. (2017)
Pasadena (US)	-118.13	34.13	0.21	Wennberg et al. (2015)
Reunion Island (FR)	55.49	-20.90	0.09	De Mazière et al. (2017)
Rikubetsu (JP)	143.77	43.46	0.36	Morino et al. (2017)
Saga (JP)	130.29	33.24	0.01	Kawakami et al. (2014)
Sodankylä (FI)	26.63	67.37	0.18	Kivi et al. (2014)
Tsukuba (JP)	140.12	36.05	0.03	Morino et al. (2018a)
Wollongong (AU)	150.88	-34.41	0.03	Griffith et al. (2014b)
Zugspitze (DE)	10.98	47.42	2.96	Sussmann and Rettinger (2018b)



**Table 2.** Definition of GOSAT/GOSAT-2 spectral fit windows (same for S and P). Windows 7 and 8 are only available for GOSAT-2. Cross sections are from HITRAN2016 except for those marked with “<sup>a</sup>”, which are from ABSCO v5.1, and those marked with “<sup>b</sup>”, which are from Gorshelev et al. (2014); Serdyuchenko et al. (2014).

No.	Primary target	Waveno. range (cm <sup>-1</sup> )	Considered gases
1	SIF	13170 – 13220	O <sub>2</sub> <sup>a</sup> , H <sub>2</sub> O <sup>a</sup> , O <sub>3</sub> <sup>b</sup>
2	O <sub>2</sub>	12930 – 13170	O <sub>2</sub> <sup>a</sup> , H <sub>2</sub> O <sup>a</sup> , O <sub>3</sub> <sup>b</sup>
3	HDO	6337 – 6410	CO <sub>2</sub> , H <sub>2</sub> O, HDO, CH <sub>4</sub>
4	CO <sub>2</sub>	6161 – 6297	CO <sub>2</sub> <sup>a</sup> , H <sub>2</sub> O, HDO, CH <sub>4</sub>
5	CH <sub>4</sub>	5945 – 6135	CO <sub>2</sub> , H <sub>2</sub> O, HDO, CH <sub>4</sub>
6	CO <sub>2</sub>	4801 – 4907	CO <sub>2</sub> <sup>a</sup> , H <sub>2</sub> O, HDO
7	N <sub>2</sub> O	4364 – 4449	N <sub>2</sub> O, H <sub>2</sub> O, HDO, CH <sub>4</sub>
8	CO	4228 – 4328	CO, H <sub>2</sub> O, HDO, CH <sub>4</sub>

**Table 3.** State vector elements and related retrieval settings. A priori values are also used as first guess. “Fit windows” lists the spectral windows (see Tab. 2) from which the element is determined. “each” means that a corresponding element is fitted in each fit window. A priori values labelled as “PP” are taken from pre-processing; “est.” denotes that they have been estimated from the background signal.

Element	Fit windows	A priori	A priori uncertainty	Comment
Gases				
co2_lay	3,4,5,6 (S&P)	PP	10.0	CO <sub>2</sub> profile (5 layers), in ppm
ch4_lay	3,4,5 (S&P)	PP	0.045	CH <sub>4</sub> profile (5 layers), in ppm
h2o_lay	3,4,5,6 (S&P)	PP	5.0	H <sub>2</sub> O profile (5 layers), in ppm
sif_fac	1 (S&P)	0.	5.	SIF spectrum scaling factor
delta_d	3,4,5,6 (S&P)	-200.	1000.	$\delta D$ profile scaling factor
n2o_scl	7 (S&P)	1.	0.1	N <sub>2</sub> O profile scaling factor, only GOSAT-2
co_scl	8 (S&P)	1.	1.0	CO profile scaling factor, only GOSAT-2
Scattering parameters				
pre_sca_s	1–6 S	0.2	1.	Layer height (pressure), S
tau_sca_0_s	1–6 S	0.01	0.1	Optical depth, S
ang_sca_s	1–6 S	4.0	1.	Ångström coefficient, S
pre_sca_p	1–6 P	0.2	1.	Layer height (pressure), P
tau_sca_0_p	1–6 P	0.01	0.1	Optical depth, P
ang_sca_p	1–6 P	4.0	1.	Ångström coefficient, P
Polynomial coefficients (surface albedo)				
poly0	each	est.	0.1	estimated surface albedo
poly1	each	0.0	0.01	
poly2	each	0.0	0.01	not in SIF window (1)
poly3	each	0.0	0.01	not in SIF window (1)
poly4	each	0.0	0.01	only in N <sub>2</sub> O window (7)
Spectral corrections				
wav_shi	each	0.0	0.1	Wavenumber shift
wav_squ	each	0.0	0.001	Wavenumber squeeze

**Table 4.** Filter settings for all products. “–” denotes that no limit is applied.

Gas	SZA Filter	$P_\tau$	$P_V$
Land			
XCO <sub>2</sub>	75°	40%	50%
XCH <sub>4</sub>	75°	40%	50%
XCH <sub>4</sub> Proxy	75°	–	20%
XH <sub>2</sub> O	–	–	30%
$\delta$ D	75°	40%	50%
XN <sub>2</sub> O	75°	40%	50%
XCO	75°	–	20%
Water			
XCO <sub>2</sub>	75°	40%	40%
XCH <sub>4</sub>	75°	40%	40%
XCH <sub>4</sub> Proxy	75°	–	20%
XH <sub>2</sub> O	–	–	30%
$\delta$ D	75°	40%	40%
XN <sub>2</sub> O	75°	40%	40%
XCO	75°	–	20%

**Table 5.** Coefficients of linear uncertainty correction.

Gas	Surface	Offset (ppm)	Slope
GOSAT			
XCO <sub>2</sub>	land	1.030937	1.27
XCO <sub>2</sub>	water	0.568207	0.83
XCH <sub>4</sub>	land	0.002487	2.07
XCH <sub>4</sub>	water	0.005121	0.83
XCH <sub>4</sub> Proxy	land	0.007951	0.67
XCH <sub>4</sub> Proxy	water	0.006026	0.59
GOSAT-2			
XCO <sub>2</sub>	land	0.292586	2.27
XCO <sub>2</sub>	water	0.596544	0.77
XCH <sub>4</sub>	land	0.004791	2.02
XCH <sub>4</sub>	water	0.006171	0.60
XCH <sub>4</sub> Proxy	land	0.008328	0.58
XCH <sub>4</sub> Proxy	water	0.006286	0.53

**Table 6.** Results from TCCON comparisons.  $N_{\text{stations}}$  denotes the number of TCCON stations involved in the comparison,  $N_{\text{data}}$  is the number of collocated data points. All products are full physics products except for those marked as ‘Proxy’.

Product (unit)	$N_{\text{stations}}$	$N_{\text{data}}$	Mean station bias	Station-to-station bias	Mean scatter	Seasonal bias
GOSAT 2009–2020 XCO <sub>2</sub> products vs. TCCON						
ACOS v9r (ppm)	24	35827	0.08	0.44	1.66	0.34
UoL v7.3 (ppm)	24	24223	0.21	0.53	1.83	0.39
SRON v2.3.8 (ppm)	24	22907	0.41	0.59	2.12	0.40
NIES v02.9xbc (ppm)	24	31323	0.61	0.54	2.02	0.40
FOCAL v3.0 (ppm)	24	32505	0.40	0.51	2.19	0.33
GOSAT 2009–2020 XCH <sub>4</sub> products vs. TCCON						
UoL v7.3 (ppb)	24	23661	-1.89	5.15	13.33	3.57
UoL Proxy v9.0 (ppb)	24	72849	-0.78	4.97	13.46	3.01
SRON v2.3.8 (ppb)	24	22907	3.24	3.64	13.39	2.92
SRON Proxy v2.3.9 (ppb)	24	74615	1.34	4.60	13.96	2.62
NIES v02.9xbc (ppb)	24	31334	-0.61	3.38	12.76	2.87
FOCAL v3.0 (ppb)	24	30245	-3.04	4.28	12.37	2.83
FOCAL v3.0 Proxy (ppb)	24	72954	-4.75	6.11	12.84	2.52
GOSAT 2009–2020 FOCAL v3.0 water vapour products vs. TCCON						
XH <sub>2</sub> O (ppm)	24	19739	-78.82	116.13	304.05	65.79
$\delta D$ (‰)	24	21892	-83.41	8.62	32.95	6.29
GOSAT-2 2019–2020 FOCAL v3.0 products vs. TCCON						
XCO <sub>2</sub> (ppm)	17	5251	-0.01	0.91	2.02	0.62
XCH <sub>4</sub> (ppb)	15	4400	-6.61	4.71	12.00	2.45
XCH <sub>4</sub> Proxy <sup>a</sup> (ppb)	15	10370	-6.02	6.15	11.19	3.05
XH <sub>2</sub> O (ppm)	14	3500	-20.89	152.47	278.41	109.91
$\delta D$ (‰)	14	2762	-82.76	8.55	31.00	12.69
XCO (ppb)	13	3777	14.80	4.32	7.67	2.84
XN <sub>2</sub> O (ppb)	11	3151	0.63	1.61	4.02	1.56

<sup>a</sup>XCH<sub>4</sub> Proxy validated together with full physics product, i.e. for same subset of TCCON stations

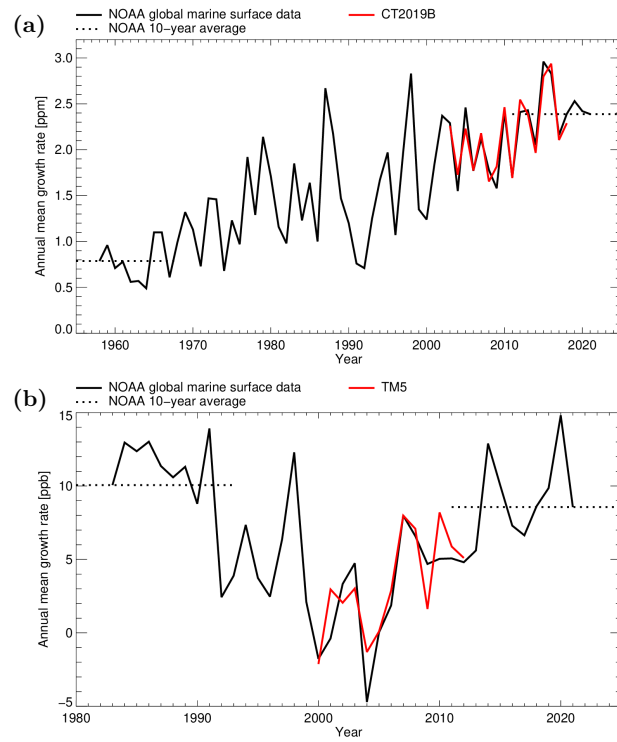


**Figure A1.** Global growth rates for CO<sub>2</sub> (a) and CH<sub>4</sub> (b).

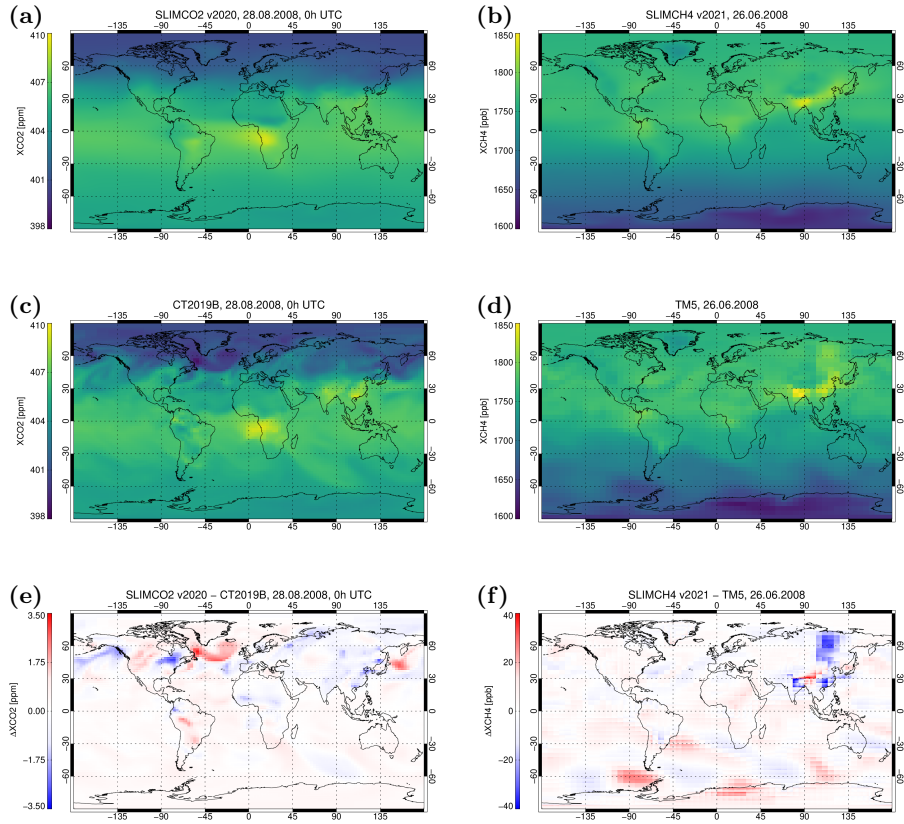


**Figure A2.** Example Maps of SLIMCO2 (a) and SLIMCH4 (b) data. Panels (c) and (d) show corresponding data from the underlying models (CT2019B, TM5). The differences between the SLIM results and these model data are shown in panels (e) and (f).

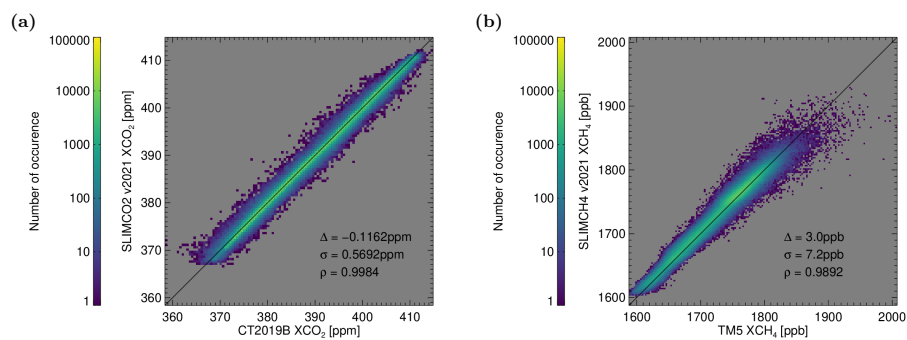


**Figure A3.** Scatter plot of the data shown in Fig. A2. (a) SLIMCO2 data vs. CT2019B. (b) SLIMCH4 vs. TM5.  $\sigma$  corresponds to the standard deviation of the difference  $\delta$  corresponds to the average bias, and  $\rho$  is the Pearson correlation coefficient.



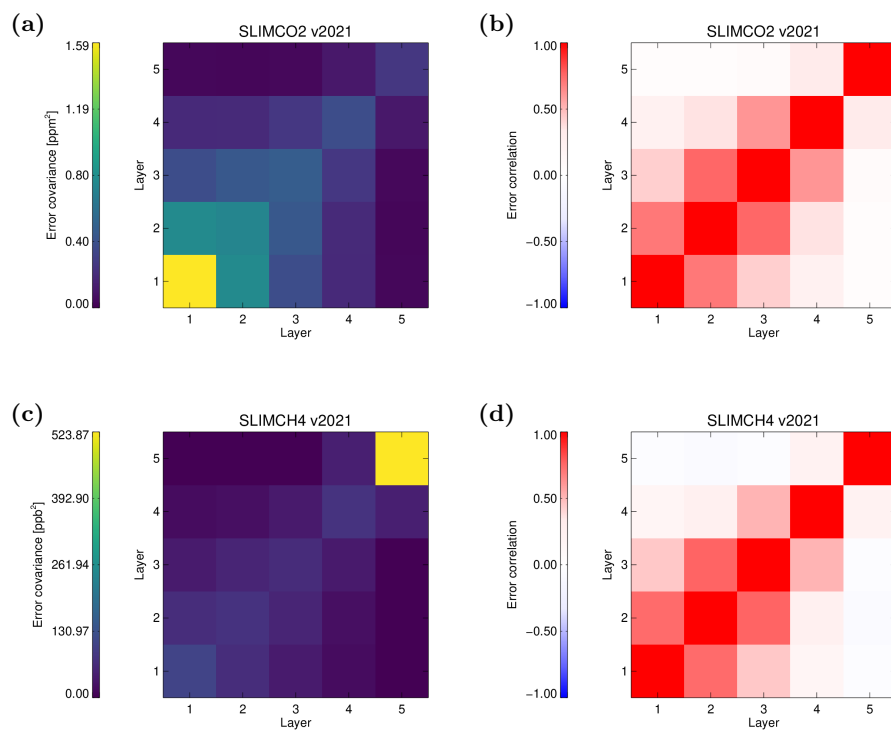


**Figure A4.** Error covariance matrices for SLIMCO2 (a) and SLIMCH4(c) and corresponding error correlation matrices (b, d).

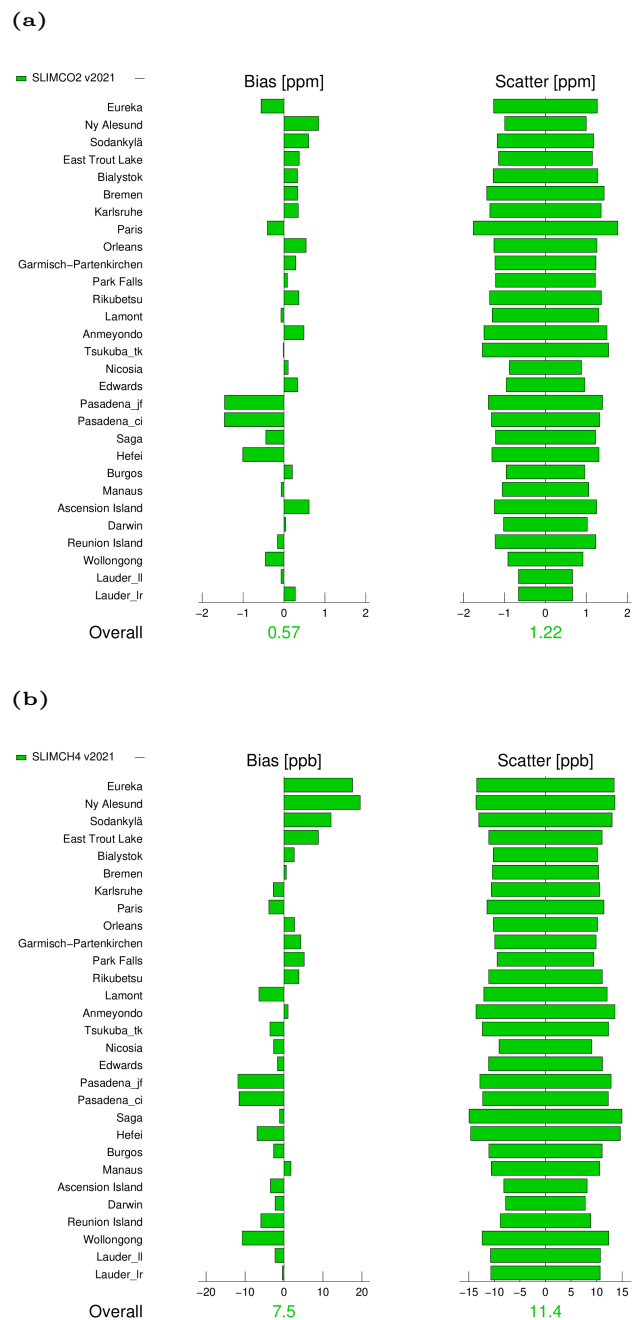


**Figure A5.** Overview of TCCON validation results for SLIMCO2 (a) and SLIMCH4 (b). The mean station bias has been subtracted to better illustrate the local station differences.

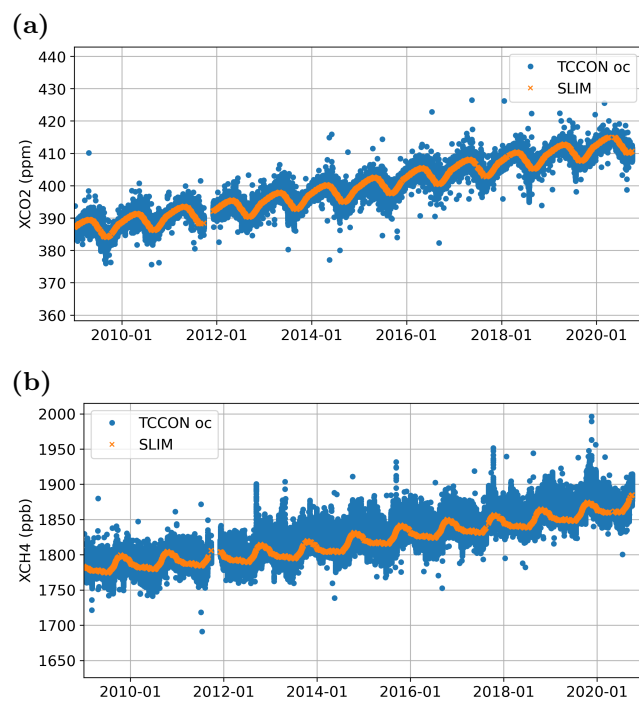


**Figure A6.** Time series of  $XCO_2$  (a) and  $XCH_4$  (b) from TCCON and SLIM at Lamont (station code oc).

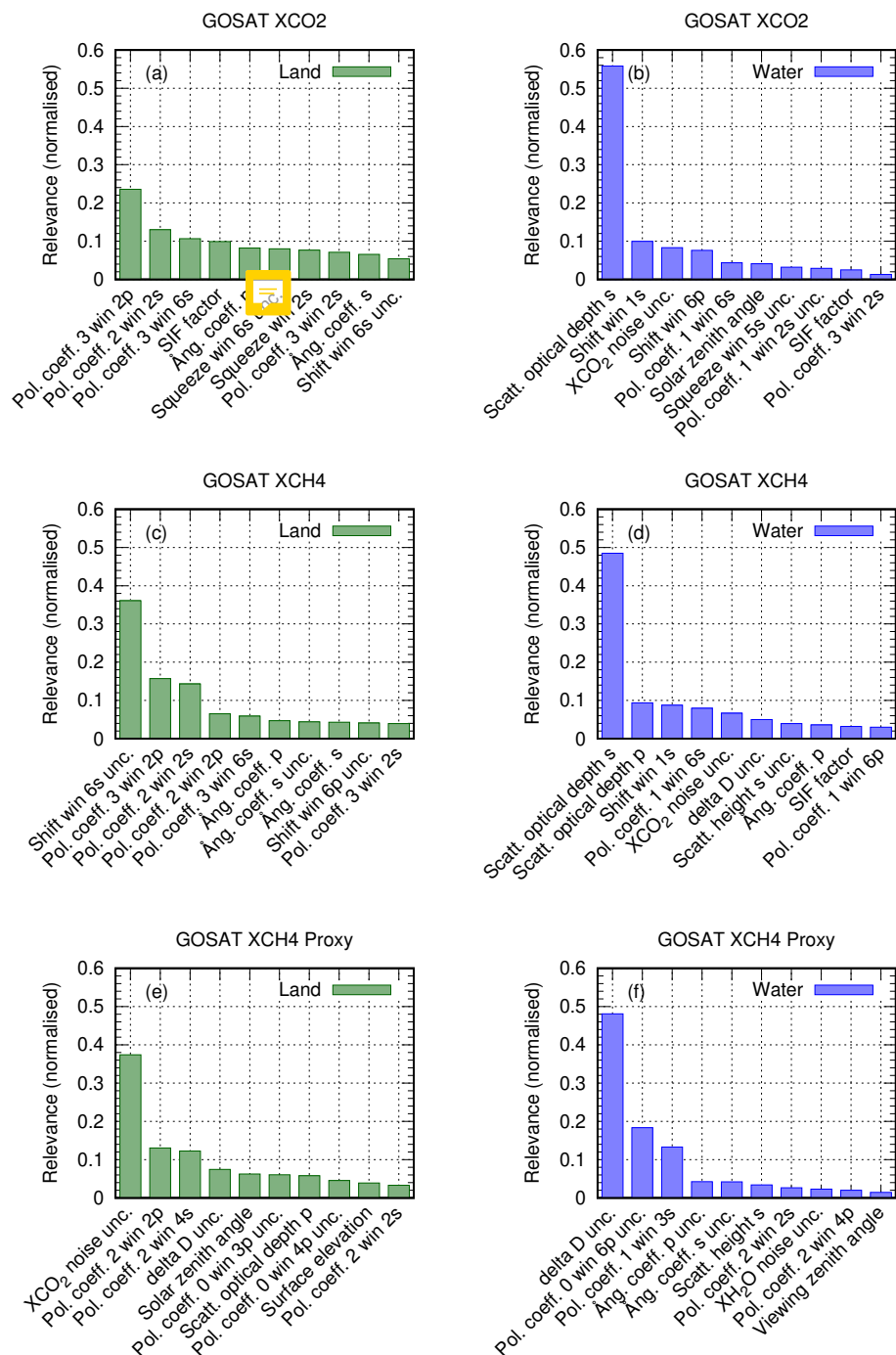



**Figure A7.** Variables selected for the GOSAT random forest bias correction and their relevance. Top: XCO<sub>2</sub>. Middle: XCH<sub>4</sub>. Bottom: XCH<sub>4</sub> Proxy. Left/right: For land/water surface.

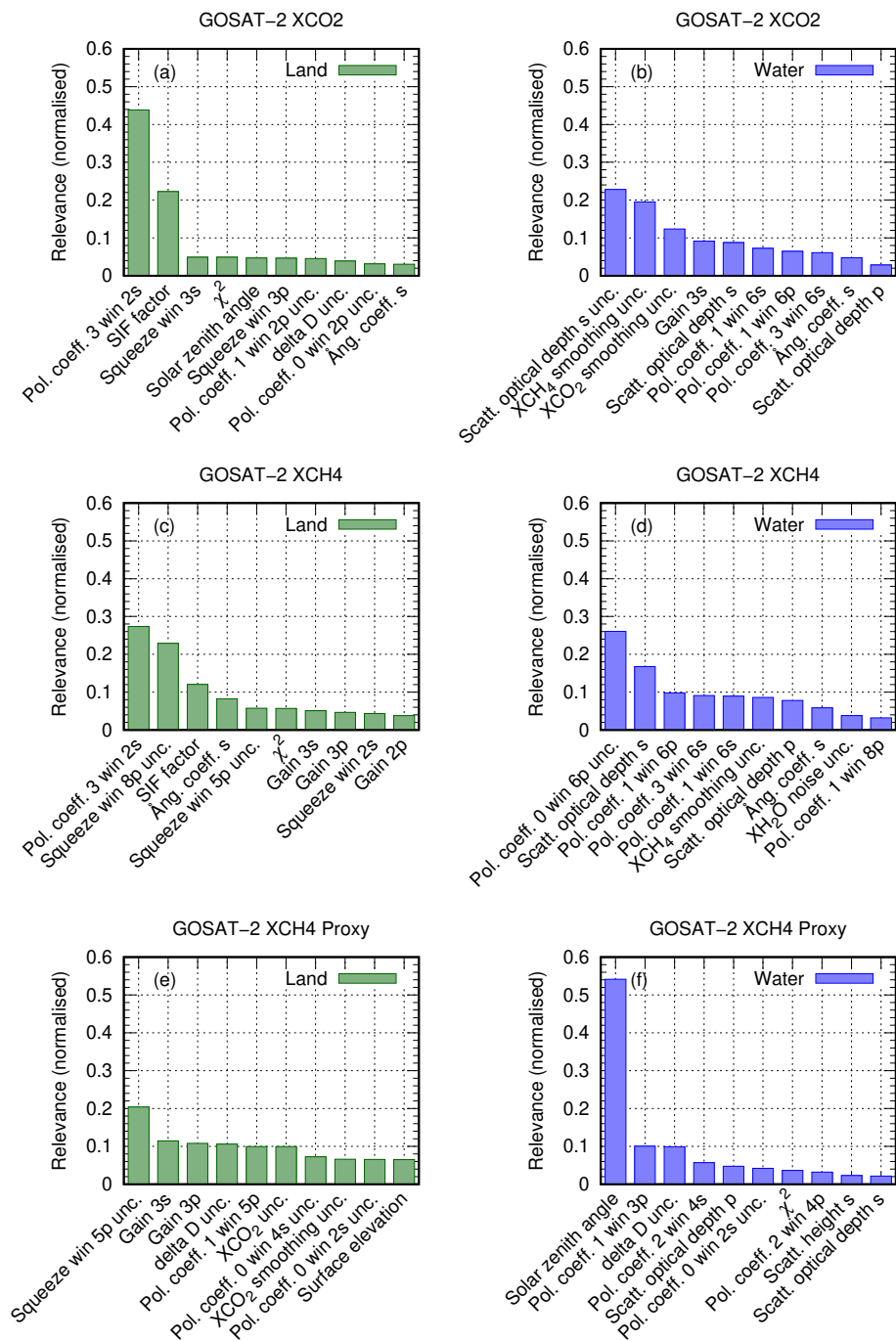


**Figure A8.** Same as Fig. A7, but for GOSAT-2.

**Table A1.** XCO<sub>2</sub> filter variables and limits for GOSAT. “–” means that no limit is applied.

Land			Water		
Variable	valid range		Variable	valid range	
	min.	max.		min.	max.
Solar zenith angle (deg)	0.00	75.00	Solar zenith angle (deg)	0.00	75.00
Scatt. optical depth s	 $1.09 \cdot 10^{-3}$	$5.37 \cdot 10^{-2}$	Scatt. optical depth p	$-7.28 \cdot 10^{-2}$	$3.53 \cdot 10^{-2}$
Scatt. optical depth p	$-5.09 \cdot 10^{-3}$	$2.80 \cdot 10^{-2}$	Scatt. optical depth s	$4.40 \cdot 10^{-3}$	$5.76 \cdot 10^{-2}$
Pol. coeff. 3 win 2s	$-6.98 \cdot 10^{-3}$	$-6.42 \cdot 10^{-5}$	Pol. coeff. 3 win 2s	–	$1.87 \cdot 10^{-3}$
Pol. coeff. 3 win 2p	$-7.32 \cdot 10^{-3}$	$2.91 \cdot 10^{-4}$	XCO <sub>2</sub> noise unc. (ppm)	0.58	1.45
Surface roughness (m)	–	54.00	Pol. coeff. 1 win 6p	$2.66 \cdot 10^{-4}$	–
XCH <sub>4</sub> noise unc. (ppm)	$3.89 \cdot 10^{-3}$	$6.58 \cdot 10^{-3}$	Pol. coeff. 1 win 5p	$8.01 \cdot 10^{-4}$	–
Scatt. Ångström coeff. p	1.07	–	Pol. coeff. 1 win 5s	$7.67 \cdot 10^{-5}$	–
Spectral squeeze win 3p	$-1.20 \cdot 10^{-3}$	$1.21 \cdot 10^{-3}$	Pol. coeff. 0 win 3s unc.	–	$3.05 \cdot 10^{-4}$
Pol. coeff. 1 win 4s	$-1.46 \cdot 10^{-2}$	$-3.05 \cdot 10^{-3}$	Pol. coeff. 0 win 4p unc.	–	$4.50 \cdot 10^{-4}$
Spectral squeeze win 3s	$-1.21 \cdot 10^{-3}$	$1.24 \cdot 10^{-3}$	δD unc. (per mille)	–	391.41
Pol. coeff. 1 win 6s	$-3.62 \cdot 10^{-3}$	–	Pol. coeff. 0 win 5s unc.	–	$5.72 \cdot 10^{-4}$
Scatt. Ångström coeff. s	$-8.71 \cdot 10^{-2}$	–	χ <sup>2</sup>	–	1.02

**Table A2.** XCH<sub>4</sub> filter variables and limits for GOSAT. “–” means that no limit is applied.

Land			Water		
Variable	valid range		Variable	valid range	
	min.	max.		min.	max.
Solar zenith angle (deg)	0.00	75.00	Solar zenith angle (deg)	0.00	75.00
Scatt. optical depth s	$-6.59 \cdot 10^{-3}$	$3.45 \cdot 10^{-2}$	Scatt. optical depth p	$-7.28 \cdot 10^{-2}$	$3.52 \cdot 10^{-2}$
Scatt. optical depth p	$2.00 \cdot 10^{-3}$	$2.80 \cdot 10^{-2}$	Scatt. optical depth s	$4.40 \cdot 10^{-3}$	$7.55 \cdot 10^{-2}$
Pol. coeff. 3 win 2p	$-7.32 \cdot 10^{-3}$	$4.12 \cdot 10^{-4}$	Pol. coeff. 3 win 2p	$-8.80 \cdot 10^{-3}$	$9.59 \cdot 10^{-5}$
Scatt. Ångström coeff. p unc.	0.16	–	Pol. coeff. 1 win 5p	$7.97 \cdot 10^{-4}$	–
Surface roughness (m)	–	55.00	Pol. coeff. 1 win 6p	$2.23 \cdot 10^{-4}$	$4.51 \cdot 10^{-3}$
Pol. coeff. 3 win 2s	$-6.98 \cdot 10^{-3}$	$4.90 \cdot 10^{-4}$	Pol. coeff. 0 win 2p unc.	–	$5.32 \cdot 10^{-4}$
Pol. coeff. 1 win 4p	–	$-4.85 \cdot 10^{-3}$	Pol. coeff. 1 win 5s	$4.26 \cdot 10^{-5}$	–
Pol. coeff. 1 win 4s	$-1.46 \cdot 10^{-2}$	$-4.99 \cdot 10^{-3}$	Pol. coeff. 0 win 5p unc.	$5.98 \cdot 10^{-5}$	$3.61 \cdot 10^{-4}$
Spectral squeeze win 5s unc.	$2.02 \cdot 10^{-4}$	$3.99 \cdot 10^{-4}$	Pol. coeff. 0 win 3s unc.	–	$2.63 \cdot 10^{-4}$
Pol. coeff. 1 win 6s	$-3.79 \cdot 10^{-3}$	–	XCO <sub>2</sub> noise unc. (ppm)	0.58	1.47
Scatt. Ångström coeff. s unc.	0.14	1.00	Pol. coeff. 0 win 5s unc.	–	$5.88 \cdot 10^{-4}$
Spectral squeeze win 3p	$-1.50 \cdot 10^{-3}$	$1.61 \cdot 10^{-3}$	Pol. coeff. 1 win 6s	$4.83 \cdot 10^{-5}$	$4.53 \cdot 10^{-3}$

**Table A3.** XCH<sub>4</sub> Proxy filter variables and limits for GOSAT. “–” means that no limit is applied.

Land			Water		
Variable	valid range		Variable	valid range	
	min.	max.		min.	max.
Solar zenith angle (deg)	0.00	75.00	Solar zenith angle (deg)	0.00	75.00
Pol. coeff. 1 win 4s	–	$-4.11 \cdot 10^{-3}$	XCO <sub>2</sub> smoothing unc. (ppm)	–	1.21
XH <sub>2</sub> O noise unc. (ppm)	–	20.08	Spectral shift win 3p unc.	–	$1.29 \cdot 10^{-3}$
XCH <sub>4</sub> noise unc. (ppm)	–	$1.48 \cdot 10^{-2}$	XCO <sub>2</sub> unc. (ppm)	–	5.14
$\chi^2$	–	0.97	XCO <sub>2</sub> noise unc. (ppm)	–	2.40
Spectral squeeze win 5s unc.	–	$5.93 \cdot 10^{-4}$	Pol. coeff. 0 win 4p unc.	$7.16 \cdot 10^{-5}$	$5.98 \cdot 10^{-4}$
Scatt. optical depth p	-0.24	0.13	Pol. coeff. 2 win 4p	–	$1.00 \cdot 10^{-4}$
Spectral squeeze win 3p	–	$1.67 \cdot 10^{-3}$	Pol. coeff. 0 win 2s	$3.64 \cdot 10^{-2}$	–
Pol. coeff. 0 win 6p unc.	–	$1.04 \cdot 10^{-3}$	$\delta D$ unc. (per mille)	–	183.57
Pol. coeff. 1 win 2p	$-7.56 \cdot 10^{-3}$	$4.48 \cdot 10^{-2}$	Scatt. Ångström coeff. s unc.	$4.11 \cdot 10^{-2}$	1.00
Pol. coeff. 1 win 4p	–	$-3.95 \cdot 10^{-3}$			



**Table A4.** XH<sub>2</sub>O filter variables and limits for GOSAT. “–” means that no limit is applied.

Land			Water		
Variable	valid range		Variable	valid range	
	min.	max.		min.	max.
$\delta D$ unc. (per mille)	26.77	–	$\delta D$ unc. (per mille)	21.29	–
Spectral squeeze win 2p unc.	$6.25 \cdot 10^{-4}$	–	XH <sub>2</sub> O noise unc. (ppm)	–	30.47
Pol. coeff. 2 win 6p unc.	$7.21 \cdot 10^{-5}$	–	Pol. coeff. 0 win 6p unc.	$1.61 \cdot 10^{-4}$	–
Pol. coeff. 0 win 2s unc.	$1.34 \cdot 10^{-4}$	–			
Pol. coeff. 0 win 5p unc.	$8.71 \cdot 10^{-5}$	–			

**Table A5.**  $\delta D$  filter variables and limits for GOSAT. “–” means that no limit is applied.

Land			Water		
Variable	valid range		Variable	valid range	
	min.	max.		min.	max.
Solar zenith angle (deg)	0.00	75.00	Solar zenith angle (deg)	0.00	75.00
Scatt. optical depth s	$1.37 \cdot 10^{-2}$	–	Scatt. optical depth s	$1.34 \cdot 10^{-2}$	$6.77 \cdot 10^{-2}$
$\delta D$ unc. (per mille)	–	36.02	Scatt. optical depth p	$1.48 \cdot 10^{-2}$	$6.18 \cdot 10^{-2}$
XH <sub>2</sub> O noise unc. (ppm)	7.27	62.48	$\delta D$ unc. (per mille)	–	38.89
XH <sub>2</sub> O unc. (ppm)	8.25	64.63	XH <sub>2</sub> O noise unc. (ppm)	9.29	104.62
SIF factor unc.	0.43	–	Pol. coeff. 1 win 1p unc.	$3.22 \cdot 10^{-4}$	$1.09 \cdot 10^{-3}$
Pol. coeff. 1 win 6p	$-9.43 \cdot 10^{-3}$	$1.65 \cdot 10^{-2}$	Pol. coeff. 1 win 6s	$-9.81 \cdot 10^{-3}$	$3.66 \cdot 10^{-3}$
Spectral squeeze win 2s unc.	$3.58 \cdot 10^{-4}$	$6.12 \cdot 10^{-4}$	Pol. coeff. 1 win 6p	$-3.13 \cdot 10^{-3}$	$3.58 \cdot 10^{-3}$

**Table A6.** XCO<sub>2</sub> filter variables and limits for GOSAT-2. “–” means that no limit is applied.

Land			Water		
Variable	valid range		Variable	valid range	
	min.	max.		min.	max.
Solar zenith angle (deg)	0.00	75.00	Solar zenith angle (deg)	0.00	75.00
Scatt. optical depth s	-0.18	$1.97 \cdot 10^{-2}$	Scatt. optical depth s	$8.82 \cdot 10^{-3}$	$2.97 \cdot 10^{-2}$
Scatt. optical depth p	$1.10 \cdot 10^{-3}$	$2.64 \cdot 10^{-2}$	Scatt. optical depth p	$7.66 \cdot 10^{-3}$	$5.41 \cdot 10^{-2}$
Scatt. Ångström coeff. p	0.56	4.52	Pol. coeff. 1 win 6s	$7.05 \cdot 10^{-5}$	$3.19 \cdot 10^{-3}$
Surface roughness (m)	–	40.00	δD unc. (per mille)	–	76.39
Scatt. Ångström coeff. s unc.	0.12	1.00	Pol. coeff. 0 win 2s unc.	$9.02 \cdot 10^{-5}$	$1.69 \cdot 10^{-4}$
Pol. coeff. 1 win 1s	–	$5.16 \cdot 10^{-3}$	Pol. coeff. 2 win 6s unc.	$4.32 \cdot 10^{-5}$	$1.58 \cdot 10^{-4}$
Spectral shift win 5s unc.	–	$3.71 \cdot 10^{-4}$	Spectral squeeze win 2s	$-3.44 \cdot 10^{-3}$	$1.48 \cdot 10^{-3}$
Scatt. Ångström coeff. s	0.71	8.21	Pol. coeff. 3 win 2p	–	$2.68 \cdot 10^{-3}$
Pol. coeff. 3 win 2s	$-1.72 \cdot 10^{-3}$	$2.48 \cdot 10^{-3}$	Scatt. Ångström coeff. s unc.	$7.11 \cdot 10^{-2}$	1.00
Spectral squeeze win 3s	$-5.96 \cdot 10^{-4}$	$1.00 \cdot 10^{-3}$	Pol. coeff. 1 win 2s	$6.70 \cdot 10^{-4}$	$8.15 \cdot 10^{-3}$
Pol. coeff. 2 win 2s unc.	$7.24 \cdot 10^{-5}$	$2.36 \cdot 10^{-4}$	Pol. coeff. 3 win 4s unc.	$2.14 \cdot 10^{-5}$	$4.89 \cdot 10^{-4}$
Spectral squeeze win 3p	$-5.67 \cdot 10^{-4}$	$1.76 \cdot 10^{-3}$	Pol. coeff. 3 win 6s unc.	$4.05 \cdot 10^{-5}$	$5.76 \cdot 10^{-4}$

**Table A7.** XCH<sub>4</sub> filter variables and limits for GOSAT-2. “–” means that no limit is applied.

Land			Water		
Variable	valid range		Variable	valid range	
	min.	max.		min.	max.
Solar zenith angle (deg)	0.00	75.00	Solar zenith angle (deg)	0.00	75.00
Scatt. optical depth s	-0.18	$1.91 \cdot 10^{-2}$	Scatt. optical depth s	$8.82 \cdot 10^{-3}$	$2.79 \cdot 10^{-2}$
Scatt. optical depth p	$-8.19 \cdot 10^{-4}$	$2.40 \cdot 10^{-2}$	Scatt. optical depth p	$3.36 \cdot 10^{-3}$	$3.59 \cdot 10^{-2}$
Scatt. Ångström coeff. s unc.	0.14	1.00	Pol. coeff. 0 win 2s unc.	$9.06 \cdot 10^{-5}$	$1.72 \cdot 10^{-4}$
Surface roughness (m)	–	40.00	Pol. coeff. 1 win 6s	$-4.19 \cdot 10^{-5}$	$3.85 \cdot 10^{-3}$
$\chi^2$	0.52	1.04	$\delta D$ unc. (per mille)	8.03	56.34
Pol. coeff. 3 win 2p	–	$5.35 \cdot 10^{-3}$	Pol. coeff. 0 win 6p	$3.34 \cdot 10^{-2}$	0.36
Scatt. Ångström coeff. p	0.17	–	Pol. coeff. 3 win 2p	–	$4.56 \cdot 10^{-3}$
XCH <sub>4</sub> unc. (ppm)	–	$5.27 \cdot 10^{-3}$	Spectral squeeze win 2s	$-2.89 \cdot 10^{-3}$	$1.41 \cdot 10^{-3}$
Pol. coeff. 1 win 4p	$-1.56 \cdot 10^{-2}$	$-4.80 \cdot 10^{-3}$	Scatt. Ångström coeff. s unc.	$8.64 \cdot 10^{-2}$	1.00
Pol. coeff. 1 win 1s	–	$4.57 \cdot 10^{-3}$	Pol. coeff. 1 win 2s	$1.78 \cdot 10^{-4}$	$1.17 \cdot 10^{-2}$
Scatt. Ångström coeff. s	0.29	8.21	Pol. coeff. 0 win 5s unc.	$4.19 \cdot 10^{-5}$	$1.53 \cdot 10^{-4}$
Pol. coeff. 3 win 2s	$-1.72 \cdot 10^{-3}$	$3.41 \cdot 10^{-3}$	Pol. coeff. 0 win 8p	$4.88 \cdot 10^{-2}$	0.28

**Table A8.** XCH<sub>4</sub> Proxy filter variables and limits for GOSAT-2. “–” means that no limit is applied.

Land			Water		
Variable	valid range		Variable	valid range	
	min.	max.		min.	max.
Solar zenith angle (deg)	0.00	75.00	Solar zenith angle (deg)	0.00	75.00
XH <sub>2</sub> O unc. (ppm)	2.84	13.70	XCO <sub>2</sub> noise unc. (ppm)	–	1.84
$\chi^2$	0.49	1.17	Pol. coeff. 0 win 5s unc.	–	$3.35 \cdot 10^{-4}$
XH <sub>2</sub> O noise unc. (ppm)	–	16.64	Pol. coeff. 0 win 8p	$3.32 \cdot 10^{-2}$	–
Pol. coeff. 0 win 4p unc.	–	$1.03 \cdot 10^{-3}$	Pol. coeff. 0 win 4s unc.	–	$5.96 \cdot 10^{-4}$
Pol. coeff. 0 win 3s unc.	$5.97 \cdot 10^{-5}$	$3.55 \cdot 10^{-4}$	XH <sub>2</sub> O noise unc. (ppm)	–	39.77
Pol. coeff. 0 win 4s unc.	$4.53 \cdot 10^{-5}$	$2.49 \cdot 10^{-4}$	Pol. coeff. 2 win 6s	$-3.26 \cdot 10^{-4}$	$3.78 \cdot 10^{-3}$
Spectral shift win 5s	$-6.64 \cdot 10^{-2}$	–	Scatt. Ångström coeff. s unc.	$3.33 \cdot 10^{-2}$	1.00
Spectral shift win 1p	-0.14	–	Pol. coeff. 1 win 2s	$-9.51 \cdot 10^{-4}$	$3.20 \cdot 10^{-2}$
Pol. coeff. 1 win 2s	$-5.63 \cdot 10^{-3}$	–			
Spectral squeeze win 8p	–	$1.12 \cdot 10^{-3}$			

**Table A9.** XH<sub>2</sub>O filter variables and limits for GOSAT-2. “–” means that no limit is applied.

Land			Water		
Variable	valid range		Variable	valid range	
	min.	max.		min.	max.
$\delta D$ unc. (per mille)	22.17	–	$\delta D$ unc. (per mille)	16.47	–
Pol. coeff. 1 win 7p unc.	$1.18 \cdot 10^{-4}$	–	XH <sub>2</sub> O noise unc. (ppm)	–	33.31
$\chi^2$	0.78	–	Pol. coeff. 0 win 3s unc.	$8.84 \cdot 10^{-5}$	–
Pol. coeff. 0 win 4s unc.	$6.86 \cdot 10^{-5}$	–	Pol. coeff. 2 win 6p unc.	$4.66 \cdot 10^{-5}$	–
Surface roughness (m)	–	177.00	XCH <sub>4</sub> smoothing unc. (ppm)	$7.52 \cdot 10^{-4}$	$3.70 \cdot 10^{-2}$
Pol. coeff. 0 win 2s unc.	$9.89 \cdot 10^{-5}$	–	Scatt. Ångström coeff. s	0.71	9.62

**Table A10.**  $\delta D$  filter variables and limits for GOSAT-2. “–” means that no limit is applied.

Land			Water		
Variable	valid range		Variable	valid range	
	min.	max.		min.	max.
Solar zenith angle (deg)	0.00	75.00	Solar zenith angle (deg)	0.00	75.00
Scatt. optical depth p	$7.70 \cdot 10^{-3}$	–	Scatt. optical depth p	$1.60 \cdot 10^{-2}$	$7.64 \cdot 10^{-2}$
$\delta D$ unc. (per mille)	–	30.24	Scatt. optical depth s	$8.81 \cdot 10^{-3}$	$5.14 \cdot 10^{-2}$
XH <sub>2</sub> O noise unc. (ppm)	6.58	52.74	$\delta D$ unc. (per mille)	–	27.86
XH <sub>2</sub> O unc. (ppm)	7.12	53.71	XH <sub>2</sub> O noise unc. (ppm)	6.78	125.86
SIF factor unc.	0.34	1.03	Pol. coeff. 3 win 2p	$-6.47 \cdot 10^{-3}$	$1.57 \cdot 10^{-3}$
Spectral squeeze win 2s unc.	$3.00 \cdot 10^{-4}$	$5.42 \cdot 10^{-4}$	Pol. coeff. 1 win 2s unc.	$8.97 \cdot 10^{-5}$	$3.38 \cdot 10^{-4}$
Pol. coeff. 1 win 6s	$-4.01 \cdot 10^{-3}$	$3.76 \cdot 10^{-3}$			

**Table A11.** XCO filter variables and limits for GOSAT-2. “–” means that no limit is applied.

Land			Water		
Variable	valid range		Variable	valid range	
	min.	max.		min.	max.
Solar zenith angle (deg)	0.00	75.00	Solar zenith angle (deg)	0.00	75.00
Scatt. Ångström coeff. s unc.	$5.45 \cdot 10^{-2}$	–	XCO unc. (ppm)	–	$8.60 \cdot 10^{-3}$
Pol. coeff. 1 win 5s	$-1.27 \cdot 10^{-2}$	$2.19 \cdot 10^{-3}$	Pol. coeff. 1 win 2s	$7.57 \cdot 10^{-4}$	$3.50 \cdot 10^{-2}$
Pol. coeff. 2 win 5s	$-1.06 \cdot 10^{-3}$	–	XH <sub>2</sub> O noise unc. (ppm)	–	22.72
Scatt. Ångström coeff. p unc.	$6.13 \cdot 10^{-2}$	–	Pol. coeff. 0 win 7s unc.	$5.40 \cdot 10^{-5}$	–
Pol. coeff. 1 win 2s	$-5.80 \cdot 10^{-3}$	–	Scatt. height s unc.	$4.99 \cdot 10^{-3}$	–
XCH <sub>4</sub> smoothing unc. (ppm)	$7.99 \cdot 10^{-4}$	–	Pol. coeff. 2 win 7s unc.	$1.41 \cdot 10^{-4}$	–
XCO unc. (ppm)	–	$9.62 \cdot 10^{-3}$	Scatt. Ångström coeff. s unc.	$3.76 \cdot 10^{-2}$	–



**Table A12.** XN<sub>2</sub>O filter variables and limits for GOSAT-2. “–” means that no limit is applied.

Land			Water		
Variable	valid range		Variable	valid range	
	min.	max.		min.	max.
Solar zenith angle (deg)	0.00	75.00	Solar zenith angle (deg)	0.00	75.00
Scatt. optical depth s	–	$1.74 \cdot 10^{-2}$	Scatt. optical depth s	–	$2.43 \cdot 10^{-2}$
Scatt. optical depth p	–	0.11	Scatt. optical depth p	–	0.11
Spectral squeeze win 6s unc.	–	$1.74 \cdot 10^{-4}$	Pol. coeff. 0 win 4s	0.11	–
Spectral squeeze win 7s unc.	–	$4.24 \cdot 10^{-4}$	Spectral squeeze win 3p unc.	–	$9.81 \cdot 10^{-4}$
Spectral shift win 7p unc.	–	$5.63 \cdot 10^{-4}$	Spectral shift win 2s unc.	–	$6.77 \cdot 10^{-4}$
Spectral squeeze win 7p unc.	–	$4.16 \cdot 10^{-4}$	Pol. coeff. 0 win 8s	$3.71 \cdot 10^{-2}$	–
Spectral shift win 8s unc.	$3.46 \cdot 10^{-4}$	$4.68 \cdot 10^{-4}$	N <sub>2</sub> O unc. (ppm)	$4.34 \cdot 10^{-3}$	$7.88 \cdot 10^{-3}$
Pol. coeff. 1 win 1s	–	$4.57 \cdot 10^{-3}$	XCO <sub>2</sub> unc. (ppm)	–	4.23
N <sub>2</sub> O unc. (ppm)	$3.90 \cdot 10^{-3}$	$9.05 \cdot 10^{-3}$	Pol. coeff. 0 win 6s	0.11	–
Scatt. Ångström coeff. s unc.	$9.32 \cdot 10^{-2}$	–	δD unc. (per mille)	–	55.78
Spectral shift win 7s unc.	–	$7.11 \cdot 10^{-4}$	Pol. coeff. 2 win 2p unc.	$1.08 \cdot 10^{-4}$	$3.24 \cdot 10^{-4}$
XCO unc. (ppm)	$2.03 \cdot 10^{-3}$	$6.25 \cdot 10^{-3}$	Pol. coeff. 1 win 8s	$2.15 \cdot 10^{-3}$	–